HIF1A contributes to the survival of aneuploid and mosaic pre-implantation embryos

Estefania Sanchez-Vasquez[1], Marianne E. Bronner[1] and Magdalena Zernicka-Goetz[1,2*]

[1]Division of Biology 139-74, California Institute of Technology, Pasadena, CA 91125, USA.
[2]Department of Physiology, Development and Neuroscience, University of Cambridge, Cambridge, UK.
*Lead and correspondence: magdaz@caltech.edu

Running title
HIF1A role in aneuploid and mosaic embryos

Key words
Embryogenesis/ Aneuploidy/ Mosaic embryos/ DNA repair/ Hypoxia

ABSTRACT

Human fertility is suboptimal, partly due to error-prone divisions in early cleavage-stages that result in aneuploidy. Most human pre-implantation are mosaics of euploid and aneuploid cells, however, mosaic embryos with a low proportion of aneuploid cells have a similar likelihood of developing to term as fully euploid embryos. How embryos manage aneuploidy during development is poorly understood. This knowledge is crucial for improving fertility treatments and reducing developmental defects. To explore these mechanisms, we established a new mouse model of chromosome mosaicism to study the fate of aneuploid cells during pre-implantation development. We previously used the Mps1 inhibitor reversine to generate aneuploidy in embryos. Here, we found that treatment with the more specific Mps1 inhibitor AZ3146 induced chromosome segregation defects in pre-implantation embryos, similar to reversine. However, AZ3146-treated embryos showed a higher developmental potential than reversine-treated embryos. Unlike reversine-treated embryos, AZ3146-treated embryos exhibited transient upregulation of Hypoxia Inducible-Factor-1A (HIF1A) and lacked p53 upregulation. Pre-implantation embryos develop in a hypoxic environment *in vivo*, and hypoxia exposure *in vitro* reduced DNA damage in response to Mps1 inhibition and increased the proportion of euploid cells in the mosaic epiblast. Inhibiting HIF1A in mosaic embryos also decreased the proportion of aneuploid cells in mosaic embryos. Our work illuminates potential strategies to improve the developmental potential of mosaic embryos.

INTRODUCTION

Humans exhibit suboptimal fertility relative to other mammals (Palmerola et al., 2022). Only ~30% of human conceptions progress to live birth (Capalbo et al., 2021). Intriguingly, the first zygotic cleavage-stage divisions in human embryos are error prone, generally resulting in aneuploidy, in which cells gain or lose chromosomes (Allais and FitzHarris, 2022; Currie et al., 2022; Palmerola et al., 2022; Pauerova et al., 2020; Vanneste et al., 2009). A high incidence of aneuploidy in the early cleavage divisions is thought to underlie low human fecundity and most developmental defects (Palmerola et al., 2022). Both *in vivo* and *in vitro* fertilization (IVF) often give rise to mosaic embryos of diploid and aneuploid cells. Although it is predicted

that ~60% of pre-implantation IVF embryos exhibit diploid-aneuploid mosaicism (Capalbo et al., 2021), our understanding of the embryo's ability to cope with such abnormalities is limited.

The incidence of aneuploidy declines at later stages of development (Shahbazi et al., 2020), but the mechanism underlying this decline is poorly understood. Human mosaic embryos can develop to term (Capalbo et al., 2021; Greco et al., 2015; Starostik et al., 2020). Specifically, implantation of low- and medium-grade mosaic embryos, defined as having 20-30% and 30-50% aneuploid extra-embryonic trophectoderm cells in a biopsy, has been reported to be as likely to result in the birth of healthy babies as implantation of fully euploid embryos (Capalbo et al., 2021). Given that some mosaic embryos are able to develop to term, it is important to uncover the mechanisms that confer their viability.

Mouse models of chromosome mosaicism enable analyses that are not allowed with human embryos for ethical reasons. Mouse and human pre-implantation development are very similar to each other: both undertake cleavage divisions, compaction, blastocyst cavity formation and hatching, albeit with slightly different timings in the two species (Mole et al., 2020; Zhu et al., 2021). During pre-implantation development, cells on the outside of the embryo form the extra-embryonic trophectoderm (TE) whereas cells on the inside form the pluripotent inner cell mass (ICM). Subsequently, cells of the ICM are segregated into the embryonic epiblast (EPI) and extra-embryonic primitive endoderm (PE). The TE will form the placenta, the PE will form the yolk sac and the EPI will form the fetus (Zhu and Zernicka-Goetz, 2020) .

Recently, our group developed the first mouse model of chromosome mosaicism, based on the generation of aneuploidies induced by a drug reversine (Bolton et al., 2016; Singla et al., 2020). Reversine is a pan-Aurora kinase inhibitor that also antagonizes the A3 adenosine receptor and inhibits mitotic kinase monopolar spindle 1 (MPS1) (D'Alise et al., 2008; Santaguida et al., 2010). Our analysis revealed that reversine-treated mosaic embryos are aneuploid and overexpress p53 (Bolton et al., 2016). Importantly, reversine-treated cells in mosaic embryos are gradually eliminated from the EPI, particularly around the time of blastocyst implantation. As with human mosaic embryos (Capalbo et al., 2021), we found that mosaic embryos with at least 50% of euploid cells had a similar developmental potential as fully euploid embryos (Bolton et al., 2016; Singla et al., 2020).

Because reversine affects p53 and may compromise cellular fitness (D'Alise et al., 2008; Santaguida et al., 2010), we sought to generate a complementary aneuploid model. To this end, we used the more specific Mps1 inhibitor, AZ3146 (Hewitt et al., 2010). Although AZ3146 and reversine both interfere with the spindle assembly checkpoint (Hewitt et al., 2010), they bind to Mps1 in a different manner (Lan and Cleveland, 2010). In mouse embryos, AZ3146 treatment was shown to double the occurrence of micronuclei, a marker of chromosome segregation defects, but without negatively affecting cellular fitness (Vazquez-Diez et al.,

2019). In the present study, we used AZ3146- and reversine-treated pre-implantation mouse embryos to dissect the mechanisms underlying aneuploid cell elimination and survival.

RESULTS

AZ3146 treatment induces chromosome segregation defects in pre-implantation mouse embryos.

To generate distinct models of aneuploidy, we treated 4- to 8-cell stage mouse embryos with AZ3146 (20 μM) (Vazquez-Diez et al., 2019), as well as with reversine (0.5 μM) (Bolton et al., 2016) as a positive control, or DMSO (vehicle) as a negative control (Fig. 1A). We evaluated how the different Mps1 inhibitors affect chromosome segregation by detecting nuclei and kinetochores in 8-cell embryos and counted chromosomes *in situ* (Pauerova et al., 2020). Micronuclei were identified as small DAPI-stained chromosomes that were clearly distinct from the nuclei. We examined 32 DMSO-treated control embryos and observed only 22 cells with micronuclei out of a total of 256 cells (Fig. S1A). In contrast, we observed 82 cells with micronuclei in a total of 144 individual cells from 18 reversine-treated embryos, and 182 cells in a total of 304 individual cells from 38 AZ3146-treated embryos. Overall, a median of 12.5% of blastomeres had micronuclei in DMSO-treated 8-cell embryos, compared to 75% of blastomeres in the reversine-treated embryos and 62.5% of blastomeres in the AZ3146-treated embryos (Fig. S1B). We also detected non-dividing nuclei as rounded circles with distinct DAPI intensities in embryos treated with reversine and AZ3146). Specifically, we observed 28 non-dividing cells (19%) in reversine-treated embryos and 24 non-dividing cells (7.9%) in AZ3146-treated blastomeres, but none in DMSO-treated blastomeres (Fig. S1B). The increased frequencies of micronuclei and non-dividing cells in response to Mps1 inhibition are consistent with elevated aneuploidy and chromosomal instability (Daughtry and Chavez, 2016; Vazquez-Diez et al., 2016), as we showed previously for reversine-treated embryos (Bolton et al., 2016).

Given these distinct responses to reversine and AZ3146, we examined how these treatments impact the lineages in the blastocyst. To this end, we treated embryos with DMSO, reversine or AZ3146 from the 4- to 8-cell stage, and then washed and cultured them until the late blastocyst stage (E4.5). We assessed lineages by immunofluorescence (IF) to detect the TE marker CDX2, the EPI marker NANOG, and the PE marker SOX17. We found that all lineages segregated normally, and that blastocyst morphology was similar in all three conditions (Fig. 1B). We quantified the number of cells in the blastocysts and found that DMSO-treated controls had a median of 93 cells in total, whereas reversine- and AZ3146-treated embryos had a median of only 79 and 82 cells, respectively (***$P<0.0001$, **$P<0.01$, *$P<0.05$, Mann–Whitney U-test, n=28 per treatment) (Fig. 1C). DMSO-treated blastocysts contained a median of 15 EPI, 11 PE, and 67 TE cells, whereas reversine-treated blastocysts contained 12 EPI, 8 PE and 59 TE cells, and AZ3146-treated blastocysts had 11 EPI, 7 PE and 64 TE cells. These data suggest that reversine treatment compromises the development of all three lineages, as observed previously (Bolton et al., 2016), whereas AZ3146 mainly compromises ICM (EPI and PE) development.

To compare the developmental potential of blastocysts that had been treated with AZ3146 or reversine, we transferred them into opposite uterine horns of the same mouse and counted decidua, which reflect successful implantation, as well as viable embryos at E9.5. Although two (8%) reversine-treated blastocysts developed decidua, none gave rise to viable E9.5 embryos (Fig. S1C). In contrast, seven (30%) AZ3146-treated blastocysts developed decidua and five (21%) generated viable E9.5 embryos (Fig. S1D). Thus, AZ3146-treated embryos appear to have a higher developmental potential than reversine-treated embryos.

Considering that cellular fitness and aneuploid stress are related to DNA damage and DNA repair, we first sought to understand if these parameters were affected in our drug treatments. We used IF to analyze the levels of the DNA repair marker PARP1 and of the DNA damage marker, phosphorylated H2A.X (γH2A.X) at the 8-cell and morula stages (Fig. 1D). We observed elevated γH2A.X levels in reversine- and AZ3146-treated 8-cell embryos compared to controls (Fig. 1D), which eventually returned to normal in AZ3146-treated blastocysts, but not in reversine-treated blastocysts (Fig. S2A).

PARP1 was specifically enriched in the EPI lineage in normal blastocysts, as assessed by IF and re-analysis of published scRNA-seq data (Deng et al., 2014) (Fig. S2B). Intriguingly, PARP1 levels were reduced at the 8-cell and morula stages in reversine-treated embryos compared to controls and to AZ3146-treated embryos (Fig. 1 D-E). Moreover, late morula stage embryos treated with the PARP inhibitor Olaparib (10 μM, Hou et al., 2022; Prasad et al., 2017) developed into smaller blastocysts with only 78 total cells, reflecting a relatively low number of ICM cells, only 8 EPI and 4 PE cells (Fig. S2C-E). Treatment with reversine, but not AZ3146, further reduced the number of cells in the EPI lineage of Olaparib-treated embryos (Fig. S2E). Overall, these data suggest that PARP1 is required for proper development of the ICM, and that its reduced levels after reversine treatment may negatively impact development.

Reversine and AZ3146 activate distinct stress response pathways in pre-implantation embryos.

Chromosome mis-segregation and aneuploidy are associated with different cellular stress pathways (Zhu et al., 2018). For instance, p53 is frequently activated following DNA damage, which can limit proliferation and trigger apoptosis (Abuetabh et al., 2022; Soto et al., 2017; Thompson and Compton, 2010). The p38 mitogen-activated protein kinase (MAPK) can also be activated following DNA damage (Thompson and Compton, 2010). In aneuploid cells, p38 promotes apoptosis by inhibiting the transcription factor Hif-1α (Simoes-Sousa et al., 2018), which otherwise promotes cell survival, proliferation, and metabolic changes in aneuploid cells and in response to hypoxia in different contexts (Hu et al., 2003; Simoes-Sousa et al., 2018).

To investigate how treatment with reversine or AZ3146 affect *p53* and *Hif1a* expression in mouse embryos, we performed RT-qPCR at the morula and blastocyst stages. We normalized to *Ppia* (Peptidylprolyl Isomerase A) mRNA, which is a stable reference gene in diploid and polyploid embryos (Gu et al., 2014).

152 Reversine-treated embryos displayed a significant increase in *p53* transcript levels at the morula (7-fold)
153 and blastocyst (1.3-fold) stages (**P<0.01, *P<0.05, Mann–Whitney U-test) (Fig. 2A), as we showed
154 previously (Singla et al., 2020). In addition, reversine-treated embryos showed reduced expression of *Hif1a*
155 at the blastocyst stage, which would be consistent with p38 activation. In contrast, AZ3146-treated embryos
156 did not show upregulation of *p53* at either the morula or blastocyst stage (Fig. 2A). Moreover, AZ3146-
157 treated embryos showed a transient increase in *Hif1a* mRNA levels (3-fold) at the morula stage compared
158 to DMSO- and reversine-treated embryos (Fig. 2A), which returned to normal levels at the blastocyst stage.
159 HIF1A protein was present in DMSO- and reversine-treated embryos, and elevated at the morula and
160 blastocyst stages in AZ3146-treated embryos (***P<0.0001, **P<0.01, *P<0.05, Mann–Whitney U-test)
161 (Fig. 2B). HIF1A appeared to be mostly nuclear in morula, but mostly cytoplasmic in blastocysts, under all
162 three conditions (Fig. 2B). Overall, these data suggest that treatment with reversine, but not AZ3146,
163 induces multiple stress pathways in pre-implantation embryos. These differences may contribute to the
164 increased developmental potential of embryos treated with AZ3146 versus reversine.
165
166 **HIF1A activity is required for proper blastocyst formation after Mps1 inhibition.**
167 It was previously shown that Hif1α$^{-/-}$ embryos undergo developmental arrest and lethality by E11 (Iyer et
168 al., 1998). To assess the role of HIF1A in the embryo's response to reversine and AZ3146, we used a
169 pharmacological approach to inhibit its function. Briefly, we tested two different small molecules that have
170 been shown to inhibit HIF1A activity, PX-478 (Lee and Kim, 2011; Zhao et al., 2015) and IDF-11774 (Ban
171 et al., 2017). We treated control zygotes with DMSO, PX-478 (2 μM), or IDF-11774 (20 μM) until the
172 blastocyst stage (Fig. S3A). Unlike PX-478, IDF-11774 treatment did not significantly affect the total number
173 of cells in the TE or the whole blastocyst compared to the control (***P<0.0001, **P<0.01, *P<0.05, Mann–
174 Whitney U-test) (Fig. S3B). Therefore, we used IDF-11774 to inhibit HIF1A in subsequent experiments.
175
176 Next, we treated embryos with DMSO, reversine, or AZ3146 from the 4- to 8-cell stage, washed them, and
177 then inhibited HIF1A with IDF-11774 from the 8-cell to blastocyst stage (Fig. 2C). Inhibition of HIF1A did
178 not abolish cavitation, but dramatically lowered the number of TE and especially PE cells in AZ3146-treated
179 embryos compared to DMSO-treated controls (Fig. 2D) and compared to AZ3146-treated embryos not
180 exposed to IDF-11884 (Fig. 1C). Inhibition of HIF1A also lowered the number of cells in reversine-treated
181 embryos compared to controls, but the effect was smaller (Fig. 2D). Overall, our data suggest that elevated
182 HIF1A activity from the 8-cell stage onwards is particularly important to promote the survival of aneuploid
183 TE and PE cells after AZ3146 treatment.
184
185 Taken together, our data suggest that AZ3146 and reversine have distinct effects on the pre-implantation
186 embryo. Compared to reversine-treated embryos, AZ3146-treated embryos appear to have increased
187 developmental potential, lack upregulation of p53, and show transient upregulation of Hif1a. Moreover,
188 AZ3146-treated embryos have a greater dependence on HIF1A activity to form the TE and PE.

Hypoxia exposure attenuates DNA damage and blastomere defects in response to Mps1 inhibition. Pre-implantation development occurs in a hypoxic environment, and many clinics culture human embryos under hypoxic conditions (Houghton, 2021). It was reported that physiologic oxygen concentrations can improve the yield and quality of mammalian blastocysts (Ciray et al., 2009; Nguyen et al., 2020) and increase the nuclear translocation of HIF1A in mouse blastocysts (Choi et al., 2021) To investigate how hypoxia affects the development of euploid and aneuploid mouse embryos, we cultured embryos from the 2-cell stage under hypoxic (5% O_2/5% CO_2) and normoxic (air, 20% O_2/5% CO_2; control) conditions until the blastocyst stage, treating them with DMSO, reversine, or AZ3146 from the 4-8 cell stage (Fig. 3A).

First, we examined lineage specification by quantifying the cell numbers in all three lineages at the blastocyst stage. We found that DMSO-treated blastocysts cultured under hypoxia had a median of 74 cells, representing 14 EPI cells, 6 PE cells and 54 TE cells (Fig. 3B-C). These data suggest that, under our conditions, the cell number in the pre-implantation mouse blastocyst is reduced when cultured in hypoxia compared to normoxia (Fig. 3C, 1C), particularly in the TE and PE. Notably, reversine and AZ3146 treatment did not further reduce cell numbers for embryos cultured under hypoxia, except for in the PE (Fig. 3C).

To investigate how hypoxia exposure affects DNA damage and repair in mouse embryos, we again performed IF for γH2A.X and PARP1 in 8-cell embryos and morula. We found that hypoxia exposure lowered the number of γH2A.X foci under all conditions, and minimized the differences between DMSO, reversine and AZ3146 treatments (Fig. 3D-E). In addition, PARP1 levels were also similar under all conditions, and relatively low in morula. Overall, these data suggest that hypoxia exposure lowers the accumulation of DNA damage under all conditions.

Hypoxia increases the proportion of euploid cells in the epiblast of mosaic blastocysts. Despite the high incidence of mosaicism in human pre-implantation embryos, the fate of aneuploid cells in mosaic embryos is incompletely understood. We previously used reversine to generate a mouse model of pre-implantation chromosome mosaicism and found that aneuploid (Reversine-treated) cells are eliminated in the EPI of mosaic embryos via apoptosis, starting from the mature blastocyst stage (Bolton et al., 2016). Whether this response reflects reversine treatment specifically, or aneuploidy more generally, is not known. Moreover, how hypoxia versus normoxia affects the outcomes is also not clear.

To address these questions, we created aggregation chimeras at the 8-cell stage that contained a 1:1 ratio of AZ3146-treated and control blastomeres (DMSO/AZ3146 chimeras), which is expected to reflect low-grade mosaicism, or of AZ3146-treated and reversine-treated blastomeres (reversine/AZ3146 chimeras), which is expected to reflect medium-grade mosaicism (Fig. 4A). We cultured these chimeric embryos in

226 normoxia and hypoxia, and followed the fate of individual blastomeres by using transgenic mouse lines with
227 the membrane markers mTmG (Muzumdar et al., 2007) and E-cadherin (Christodoulou et al., 2019).
228 DMSO/AZ3146 and reversine/AZ3146 blastocysts displayed proper lineage allocation, embryo morphology
229 and cavitation in both normoxia and hypoxia (Fig. 4B-C). In addition, DMSO/AZ3146 and reversine/AZ3146
230 embryos had comparable total cell numbers in their blastocysts, and blastocysts grown in hypoxia were
231 again smaller than those grown in normoxia (Fig. 4D-E). Intriguingly, despite having fewer total cells,
232 DMSO/AZ3146 blastocysts had more EPI cells when they were cultured in hypoxia compared to normoxia
233 (Fig. 4D-E).
234
235 We quantified the proportion of AZ3146 cells in each lineage for each chimera. In DMSO/AZ3146-treated
236 blastocysts, we found that 46.75% of the TE and 42.88% of the EPI originated from AZ3146-treated
237 blastomeres, compared to only 28.57% of the PE (Fig. 4F). In reversine/AZ3146 chimeras, 63% of the TE
238 and 78.4% of the EPI originated from AZ3146-treated cells, compared to only 40% of the PE (Fig. 4G).
239 Thus, under normoxia, DMSO cells appear to outcompete AZ3146-treated cells, which in turn outcompete
240 Reversine-treated cells in the TE and EPI. AZ3146-treated cells appeared to be at a competitive
241 disadvantage in the PE in both contexts. Culturing DMSO/AZ3146 chimeras in hypoxia slightly increased
242 the representation of AZ3146-treated blastomeres in the TE (49.06%) and PE (50%) but, strikingly, reduced
243 their representation in the EPI (33.3%) (Fig. 4G). These altered frequencies reflect a higher number of
244 DMSO-treated cells in the EPI and a lower number in the PE (Fig. 4E). Hypoxia exposure of
245 reversine/AZ3146 embryos lowered the contribution of AZ3146-treated blastomeres to the TE (55.94%)
246 and EPI (50%) but not the PE (46.43%) (Fig. 4G). We found that there was no correlation between the
247 proportion of AZ3146-treated cells in the TE and the EPI in DMSO/AZ3146 and reversine/AZ3146 chimeras,
248 under hypoxia or normoxia, and that hypoxia seemed to have a greater impact on the proportion of AZ3146
249 cells in reversine/AZ3146 chimeras (Fig. S4). Overall, these data suggest that hypoxia has lineage-specific
250 effects on competitions between aneuploid and euploid cells and increases the contribution of euploid cells
251 to the EPI.
252
253 Blastomeres in the 4-cell stage embryo display a lineage bias (Goolam et al., 2016). We considered that
254 mosaicism generated before the 4-cell stage might influence lineage allocation. To test this possibility, we
255 treated zygotes with reversine or AZ3146 during the first cell division. Importantly, reversine treatment at
256 the 2-cell stage seems to strongly affect the morphology of the blastocysts (Fig. S5A). Consistent with this
257 change in morphology, reversine-treatment reduced the number of cells in all lineages, particularly in the
258 TE and PE (Fig. S5B). In contrast, AZ3146 treatment did not affect morphology or cell number in any of the
259 lineages (Fig. S5A-B) ($n>27$ per treatment, ***$P<0.0001$, **$P<0.01$, *$P<0.05$, Mann–Whitney U-test). To
260 evaluate how early generation of aneuploidies in the embryos affect cell competition, we generated
261 DMSO/AZ3146, reversine/DMSO, and AZ3146/reversine aggregation chimeras at the 2-cell stage and
262 cultured them under normoxia until the blastocyst stage (Fig. S5C). We found that all three 2-cell stage

263 aggregation chimeras developed into blastocysts with a normal morphology and cavitation (Fig. S5D).
264 Interestingly, the reversine-treated cells were extruded from the blastocyst in 54% of the reversine/DMSO
265 chimeras and in 33% of the AZ3146/reversine chimeras, whereas no cell extrusion was observed in the
266 DMSO/AZ3146 chimeras. Quantification of the proportion of AZ3146-treated cells in 2-cell stage derived
267 chimeras showed similar results as 8-cell stage derived chimeras (Fig. S5E). In DMSO/AZ3146-treated
268 blastocysts, we found that 49.28% of the TE, 39% of the EPI and 33.33% of the PE originated from AZ3146-
269 treated blastomeres (Fig. S5E). In reversine/AZ3146 chimeras, 68.24% of the TE, 68.83% of the EPI, and
270 66.67% of the PE originated from AZ3146-treated cells (Fig. S5E). In DMSO/reversine chimeras, 22.27%
271 of the TE, 26.98% of the PE, and 31.7% of the EPI originated from reversine-treated cells. Overall, these
272 results suggest that aneuploidy generated at different stages similarly affect the proportion of aneuploid
273 cells in the blastocysts.
274
275 **HIF1A inhibition reduces the frequency of aneuploid cells in DMSO/AZ3146 mosaic embryos.**
276 Our data suggest that hypoxia affects aneuploid-euploid cell competition in mosaic embryos (Fig. 4). To
277 further assess the effect of HIF1A and, considering most human embryos are culture under hypoxic
278 conditions, we decided to evaluate the effect of inhibiting HIF1A in mosaic embryos cultured in hypoxic
279 conditions. We assembled DMSO/AZ3146 and AZ3146/reversine 8-cell stage chimeras, treated them with
280 the HIF1A inhibitor IDF-11774 (Fig. 5A, S6A-B), and then assessed lineage allocation in blastocysts.
281 Treatment of DMSO/AZ3146 chimeras with IDF11774 reduced the cavitation diameter and diminished the
282 contribution of AZ3146-treated cells to all three lineages, and DMSO-treated cells compensated for this
283 loss in the PE and EPI (Fig. 5B-D, Fig. S6C). Treating AZ3146/reversine chimeras with IDF11774
284 compromised blastocyst morphology (Fig. 5E-F) and slightly increased the number of PE and EPI cells
285 (Fig. 5G), without altering the frequency of AZ3146-treated cells (Fig. S6D). Taken together, our data
286 suggest that HIF1A promotes the survival of AZ3146-treated cells in DMSO/AZ3146 chimeras, and suggest
287 that inhibiting HIF1A could increase the proportion of karyotypically normal cells in mosaic embryos.
288
289 **DISCUSSION**
290 Aneuploidy is a common event during pre-implantation development (Allais and FitzHarris, 2022; Currie et
291 al., 2022; Palmerola et al., 2022). Here, we describe different strategies to generate aneuploidy in the early
292 embryo. Our results suggest that: 1) the Mps1 inhibitor, AZ3146, generates aneuploid embryos with
293 enhanced DNA repair and reduced stress responses when compared to reversine-treated embryos. 2)
294 Lineage specific responses to aneuploidy are present during blastocyst development, as we showed
295 previously (Bolton et al., 2016; Singla et al., 2020). 3) HIF1A contributes to the survival of TE and PE cells
296 in AZ3146-treated embryos whereas PARP1 is particularly required in EPI cells in both reversine and
297 AZ3146-treated embryos. 4) Hypoxia enhances DNA repair and affects aneuploid-euploid cell competition
298 in mosaic embryos.
299

300 Reversine-treated mouse embryos upregulate the senescent markers p53 and p21 (Singla et al., 2020) and
301 fail to give rise to viable embryos (Bolton et al., 2016). Our results further indicate that reversine
302 downregulates PARP1, as previously observed in glioma (Hirakata et al., 2021). Thus, reversine treatment
303 may compromise embryo development due to a combined increase in DNA damage and decrease in DNA
304 repair. In contrast, embryos treated with AZ3146 do not reduce PARP1 levels and have elevated HIF1A,
305 which appears to improve survival of TE and PE cells and developmental potential.
306
307 DNA repair pathways are enhanced under hypoxic environments in somatic cells (Marti et al., 2021;
308 Nakamura et al., 2022; Pietrzak et al., 2018). Similarly, our data show that aneuploid embryos cultured in
309 hypoxia had lower levels of DNA damage at the morula stage, in agreement with previous studies reporting
310 lower levels of γH2A.X in mouse blastocysts recovered from the uterus and in blastocysts cultured in
311 hypoxia compared to blastocysts cultured in normoxia (Houghton, 2021; Meuter et al., 2014). Interestingly,
312 recent studies suggest that hypoxia favors HIF1A's association with PARP1 in cancer cells, increasing DNA
313 repair (Marti et al., 2021; Nakamura et al., 2022; Pietrzak et al., 2018). In the future, a deeper understanding
314 of the regulation of DNA repair in pre-implantation stages would allow us to understand the molecular
315 response of embryos to aneuploid stress.
316
317 Confined placental mosaicism is commonly observed in human pregnancies, and refers to instances where
318 the placenta is aneuploid but the fetus is euploid (McCoy, 2017). We previously found that aneuploid TE
319 cells have an increased cell cycle length and senescence, whereas aneuploid ICM cells have an increased
320 frequency of apoptosis, in reversine-treated embryos. Therefore abnormal but viable TE cells could lead to
321 confined placental mosaicism. Our results further suggest that aneuploid cells contributed mostly to the TE,
322 followed by the EPI, are especially depleted from the PE in AZ3146-treated embryos under normoxia.
323 Intriguingly, under hypoxia aneuploid cells were depleted from the EPI and increase in the PE. Overall our
324 data suggest that hypoxia may affect cell competition in a lineage-specific manner in the pre-implantation
325 embryo, supporting an increased representation of euploid cells in the EPI relative to the PE and TE.
326
327 Finally, our results confirm that the proportion of aneuploid cells in the EPI and TE do not correlate,
328 consistent with aneuploid survival in the TE but elimination from the ICM. These results are not surprising
329 considering the low aneuploidy concordance rates between TE and ICM in human mosaic aneuploid
330 embryos (30–40%) (Dahdouh and Garcia-Velasco, 2021).
331
332 Since low- and medium- grade mosaic human embryos have similar developmental potential as fully
333 euploid embryos (Capalbo et al., 2021; Greco et al., 2015), understanding the molecular pathways involved
334 in the responses to aneuploidy may have translational implications. Given that the extent and proportion of
335 aneuploid cells in mosaic embryos impact survival (Capalbo et al., 2021), we propose that a reduction in
336 aneuploid cells in the blastocyst will favor a successful pregnancy. Here, we downregulated HIF1A as a

337 strategy for reducing aneuploid cells number and found that treatment with IDF-11774 increased the
338 proportion of euploid cells in mosaic embryos. In sum, our study reveals distinct environmental factors that
339 affect the extent and proportion of aneuploid cells within mosaic embryos.
340
341 **MATERIALS AND METHODS**
342 **Pre-implantation embryo culture**
343 Mice were maintained according to national and international guidelines. Four- to six-week-old B6SJLF1/J
344 female mice were injected with 7.5IU PMSG followed by 7.5 IU hCG 48 h later, to induce superovulation.
345 The females were then mated with B6CBAF1/J males or were indicated, with E-cadherin GFP or mTmG
346 transgenic males. Pre-implantation mouse embryos were recovered 24 h and 40 h after the hCG injection
347 to obtain zygotes and 2-cell stage embryos, respectively in M2 medium (Sigma, M7167). We incubate the
348 embryos in KSOM until 4-cell stage for the aneuploid treatment, around 53 h post hCG. When recovering
349 zygotes, cumulus cells were removed with 0.3% hyaluronidase (Sigma, H4272) in M2. Embryos then were
350 cultured in regular KSOM (Sigma. MR-106) at 37°C under 5% CO_2/air (Normoxia) or with pre-mixed 5%
351 CO_2/ 5% O_2 balance with nitrogen, biologic atmosphere batch (Airgas #Z03NI9022000033)(Hypoxia).
352 B6SJLF1/J females and B6CBAF1/J males were obtained from JAX laboratories. Females were received
353 at 3-4 weeks of age and were maintained in the CALTECH animal facility, where they were housed with 5
354 same-sex littermates on a 12 h light/12 h dark cycle with food and water *ad libitum*. The temperature in the
355 facility was controlled and maintained at 21 °C. All experimental procedures involving the use of live
356 animals, or their tissues were performed in accordance with the NIH guidelines and approved by the
357 Institutional Animal Care and Use Committee (IACUC) and the Institutional Biosafety Committee at the
358 California Institute of Technology (CALTECH). Reversine (Sigma, R3904), AZ3146 (Sigma, SML1427), PX-
359 478 (Selleckchem, S7612), IDF-11774 (Selleckchem, S8771) and olaparib (Selleckchem, S1060) were
360 dissolved in DMSO (Sigma, D2650) before use to specific concentration. They were respectively used at
361 following final concentrations: 0.5 μM, 20 μM, 2 μM, 20 μM and 10 μM. Control embryos were incubated in
362 the equivalent DMSO concentration. Drugs were dissolved in regular KSOM to the concentration of use.
363 DMSO concentration in media should never pass 0.4%.
364
365 **Immunofluorescence**
366 Embryos were fixed in 4% PFA (Thermo Scientific, AA47340) for 20 min at room temperature (RT).
367 Following by three washes with 0.1% Tween-20 (Sigma, P1379) dissolved in PBS (PBST). The embryos
368 were then permeabilized with 0.3%, Triton X-100 (Sigma, X100) in PBS. Washes were then performed
369 three times in PBST before embryos were transferred to blocking solution (3% BSA in PBS) for at least 3h
370 at RT. Incubation with primary antibodies was performed in blocking solution overnight at 4°C. Next day,
371 washes were performed three times in PBST before incubation with Alexa Fluor secondary antibodies
372 (Thermo Fisher Scientific, 1:500) in blocking solution for 2 h. Washes were performed three times before
373 incubation with DAPI (Thermo Fisher Scientific) for 5 min. Washes after DAPI were perform two times in

374 PBST before the final incubation in M2. Embryos were then mounted in M2 micro-drops on 35 mm glass
375 bottom dish (MATTEK, P35G-1.5-14-C). Confocal imaging was carried out using Leica SP8, 40x objective,
376 1 μM Z-step. Image files were viewed and analyzed using ImageJ and IMARIS 9.9 software.
377 Primary antibodies used: mouse anti-CDX2 (Biogenex, 1:500), rabbit anti-NANOG (1:500; Abcam), goat
378 anti-SOX17 (1:300; R&D Systems), rabbit anti-HIF1A (1:300, Novusbio), mouse anti-PARP1 (1:500,
379 Proteintech) and rabbit anti- Phospho- Histone H2AX (1:500, R&D Systems).
380
381 ***In situ* chromosome counting**
382 For determination of aneuploidy, treated 8-cell stage embryos were synchronized in metaphase by 10h
383 treatment with 0.03 μg/mL colcemid (Cayman, 15364) diluted in KSOM. Following by 1h treatment with 10
384 μM Mg132 (Selleckchem, S2619) in KSOM. Finally, 1 h treatment with 5 μM dimethylenastron
385 (MedChemExpress, HY-19944) and 10 μM Mg132 in KSOM. Synchronized embryos were then fix in 2%
386 PFA for 20 min, permeabilized with PBST for 15 min and blocked 3h at RT before incubation with human
387 anti-centromere protein antibody (1:300, Antibodiesinc 15-234) overnight at 4°C. Next day, three washes
388 with PBST were performed before 2 h incubation with goat anti-Human secondary antibody, Alexa Fluor
389 647 (1:400, Invitrogen A-21445) in blocking solution. Washes were performed three times before 20 min
390 incubation with DAPI (1:500) and Alexa Fluor 488 Phalloidin (1:300, Invitrogen A12379). Washes then were
391 performed three times before clearing overnight with AF1 plus (Citifluor, AF1/DAPI-15). Embryos were then
392 mounted in AF1 plus micro-drops on 35 mm glass bottom. Confocal imaging was carried out using Leica
393 SP8, 60x objective, 0.5 μM Z-step. Image files were viewed and analyzed using ImageJ and IMARIS 9.9
394 software.
395
396 **Embryo transfers and post implantation recovery and biopsy**
397 Embryo transfer were performed as described previously(Bermejo-Alvarez et al., 2014). CD1 females and
398 vasectomizes CD1 males were obtained from Charles River. Reversine and AZ3146-treated blastocyst
399 were transfer into 2.5-days pseudopregnant CD1 females. Around 16 AZ3146-treated embryos were
400 transfer in the right uterine horn, whereas around 16 reversine-treated embryos were transfer in the left
401 uterine horn of the same female as control. To evaluate implantation and embryo survival potency, uterine
402 horns were recovered 5 days after surgery. Deciduas were dissected and post implantation embryos at
403 stage E9.5 were recovered into PBST on ice. Embryos were fixed in 4% PFA at RT for 1 h, followed by
404 washes through PBST before imaging. Images were taken using an Olympus LS stereo microscope with a
405 10x objective. Uterine transfers were performed in accordance with the NIH guidelines and approved by
406 the Institutional Animal Care and Use Committee (IACUC) and the Institutional Biosafety Committee at the
407 California Institute of Technology (CALTECH).
408
409 **qRT-PCR**

410 Around 14 to 17 morulas and blastocysts were collected for quantitative reverse transcriptase polymerase
411 chain reaction (qRT-PCR). Total RNA from morulas was obtained using the NucleoSpin RNA Plus XS kit
412 (Takara, 740990.10). Whereas total RNA from blastocyst was extracted using the Arcturus PicoPure RNA
413 Isolation Kit (Thermo Fisher, KIT0204). qRT-PCR was performed using the *Power* SYBR Green RNA-to-
414 CT 1-Step Kit (Applied Biosystems, 4389986) in a StepOne Plus Real-time PCR machine (Applied
415 Biosystems). The following program was used: 30 min 48 °C (reverse-transcription) followed by 10 min 95
416 °C followed by 45 cycles of 15 s 95 °C (denaturing) and 1 min 60 °C (annealing and extension). The ddCT
417 method was used to determine relative levels of mRNA expression, with Ppia as an endogenous control(Gu
418 et al., 2014). Primers were obtained from IDT.

Name	**Sequence**
p53_Fw	GTCACAGCACATGACGGAGG
p53_Rv	TCTTCCAGATGCTCGGGATAC
Hif1a_Fw	CCTGCACTGAATCAAGAGGTTGC
Hif1a_Rv	CCATCAGAAGGACTTGCTGGCT
Ppia_Fw	GAGCTCTGAGCACTGGAGAGA
Ppia_Rv	CCACCCTGGCACATGAAT

419

420 **Generation of chimeric embryos**

421 Chimeric embryos were generated following a previous publish protocol(Eakin and Hadjantonakis, 2006).
422 Briefly, wild-type, E-cadherin GFP or mTmG 8-cell stage embryos were transfer to micro-drops of M2 after
423 aneuploid treatment. Zona pellucida was removed by treatment with acidic Tyrode's solution (Sigma,
424 T1788). The embryos were then incubated in Ca2+/Mg2+-free M2 (made in house) for 5 min and then
425 disaggregated into individual blastomeres by gentle mouth pipetting. Low-grade mosaic chimeras were
426 form by aggregation of four and four (1:1) of DMSO/reversine-treated blastomeres with AZ3146-treated
427 blastomeres, respectively in KSOM. Medium-grade mosaic chimeras were form by aggregation of three
428 DMSO-treated blastomeres, three AZ3146-treated blastomeres and two reversine-treaded blastomeres in
429 KSOM. Culture of the chimeras were performed under normoxic and hypoxia condition in KSOM for 48 h
430 to reach blastocyst stage.

431 **Statistical analysis**

432 The statistical tests used are indicated in the corresponding figure legends. Calculations were carried out
433 in Microsoft Excel and data analysis and visualization in Prism 9 software. All graphs show mean values,
434 error bars: s.e.m.

435

436 **AUTHOR CONTRIBUTIONS**

437 E.S.V designed and conducted the experiments; analyzed and interpreted the data. E.S.V and M.Z.G
438 conceived the project. M.E.B and M.Z.G supervised the study.

439

ACKNOWLEDGEMENTS

This work was supported by M.Z.G' National Institutes of Health R01 (R01HD101489) grant. E.S.V. is supported by a Pew Latin America fellowship. We thank the Life Science Editors and the Life Science Editors Foundation for invaluable comments and suggestions on the manuscript, and Ariane Helou for copy editing. Data analysis was performed in the Biological Imaging Facility, with the support of the Caltech Beckman Institute and the Arnold and Mabel Beckman Foundation.

DECLARATION OF INTERESTS

The authors declare that they have no conflicts of interest.

REFERENCES

Abuetabh, Y., Wu, H. H., Chai, C., Al Yousef, H., Persad, S., Sergi, C. M. and Leng, R. (2022). DNA damage response revisited: the p53 family and its regulators provide endless cancer therapy opportunities. *Exp Mol Med* **54**, 1658-1669.

Allais, A. and FitzHarris, G. (2022). Absence of a robust mitotic timer mechanism in early preimplantation mouse embryos leads to chromosome instability. *Development* **149**.

Ban, H. S., Kim, B. K., Lee, H., Kim, H. M., Harmalkar, D., Nam, M., Park, S. K., Lee, K., Park, J. T., Kim, I., et al. (2017). The novel hypoxia-inducible factor-1alpha inhibitor IDF-11774 regulates cancer metabolism, thereby suppressing tumor growth. *Cell Death Dis* **8**, e2843.

Bermejo-Alvarez, P., Park, K. E. and Telugu, B. P. (2014). Utero-tubal embryo transfer and vasectomy in the mouse model. *J Vis Exp*, e51214.

Bolton, H., Graham, S. J. L., Van der Aa, N., Kumar, P., Theunis, K., Fernandez Gallardo, E., Voet, T. and Zernicka-Goetz, M. (2016). Mouse model of chromosome mosaicism reveals lineage-specific depletion of aneuploid cells and normal developmental potential. *Nature communications* **7**, 11165.

Capalbo, A., Poli, M., Rienzi, L., Girardi, L., Patassini, C., Fabiani, M., Cimadomo, D., Benini, F., Farcomeni, A., Cuzzi, J., et al. (2021). Mosaic human preimplantation embryos and their developmental potential in a prospective, non-selection clinical trial. *Am J Hum Genet* **108**, 2238-2247.

Chi, F., Sharpley, M. S., Nagaraj, R., Roy, S. S. and Banerjee, U. (2020). Glycolysis-Independent Glucose Metabolism Distinguishes TE from ICM Fate during Mammalian Embryogenesis. *Developmental cell* **53**, 9-26 e24.

Choi, J., Kim, W., Yoon, H., Lee, J. and Jun, J. H. (2021). Dynamic Oxygen Conditions Promote the Translocation of HIF-1alpha to the Nucleus in Mouse Blastocysts. *BioMed research international* **2021**, 5050527.

Christodoulou, N., Weberling, A., Strathdee, D., Anderson, K. I., Timpson, P. and Zernicka-Goetz, M. (2019). Morphogenesis of extra-embryonic tissues directs the remodelling of the mouse embryo at implantation. *Nat Commun* **10**, 3557.

Ciray, H. N., Aksoy, T., Yaramanci, K., Karayaka, I. and Bahceci, M. (2009). In vitro culture under physiologic oxygen concentration improves blastocyst yield and quality: a prospective randomized survey on sibling oocytes. *Fertil Steril* **91**, 1459-1461.

Currie, C. E., Ford, E., Benham Whyte, L., Taylor, D. M., Mihalas, B. P., Erent, M., Marston, A. L., Hartshorne, G. M. and McAinsh, A. D. (2022). The first mitotic division of human embryos is highly error prone. *Nat Commun* **13**, 6755.

D'Alise, A. M., Amabile, G., Iovino, M., Di Giorgio, F. P., Bartiromo, M., Sessa, F., Villa, F., Musacchio, A. and Cortese, R. (2008). Reversine, a novel Aurora kinases inhibitor, inhibits colony formation of human acute myeloid leukemia cells. *Mol Cancer Ther* **7**, 1140-1149.

Dahdouh, E. M. and Garcia-Velasco, J. A. (2021). Embryos with mosaic results: busting the myth! *Reprod Biomed Online* **43**, 1-2.

489 **Eakin, G. S. and Hadjantonakis, A. K.** (2006). Production of chimeras by aggregation of embryonic stem
490 cells with diploid or tetraploid mouse embryos. *Nat Protoc* **1**, 1145-1153.
491 **Goolam, M., Scialdone, A., Graham, S. J. L., Macaulay, I. C., Jedrusik, A., Hupalowska, A., Voet, T.,**
492 **Marioni, J. C. and Zernicka-Goetz, M.** (2016). Heterogeneity in Oct4 and Sox2 Targets Biases
493 Cell Fate in 4-Cell Mouse Embryos. *Cell* **165**, 61-74.
494 **Greco, E., Minasi, M. G. and Fiorentino, F.** (2015). Healthy Babies after Intrauterine Transfer of Mosaic
495 Aneuploid Blastocysts. *N Engl J Med* **373**, 2089-2090.
496 **Gu, Y., Shen, X., Zhou, D., Wang, Z., Zhang, N., Shan, Z., Jin, L. and Lei, L.** (2014). Selection and
497 expression profiles of reference genes in mouse preimplantation embryos of different ploidies at
498 various developmental stages. *PLoS One* **9**, e98956.
499 **Hewitt, L., Tighe, A., Santaguida, S., White, A. M., Jones, C. D., Musacchio, A., Green, S. and**
500 **Taylor, S. S.** (2010). Sustained Mps1 activity is required in mitosis to recruit O-Mad2 to the
501 Mad1-C-Mad2 core complex. *J Cell Biol* **190**, 25-34.
502 **Hirakata, C., Lima, K., De Almeida, B. O., De Miranda, L. B. L., Florencio, K. G. D., Furtado, L. C.,**
503 **Costa-Lotufo, L. V. and Machado-Neto, J. A.** (2021). Targeting glioma cells by antineoplastic
504 activity of reversine. *Oncol Lett* **22**, 610.
505 **Houghton, F. D.** (2021). HYPOXIA AND REPRODUCTIVE HEALTH: Hypoxic regulation of
506 preimplantation embryos: lessons from human embryonic stem cells. *Reproduction* **161**, F41-F51.
507 **Hu, C. J., Wang, L. Y., Chodosh, L. A., Keith, B. and Simon, M. C.** (2003). Differential roles of hypoxia-
508 inducible factor 1alpha (HIF-1alpha) and HIF-2alpha in hypoxic gene regulation. *Mol Cell Biol* **23**,
509 9361-9374.
510 **Iyer, N. V., Kotch, L. E., Agani, F., Leung, S. W., Laughner, E., Wenger, R. H., Gassmann, M.,**
511 **Gearhart, J. D., Lawler, A. M., Yu, A. Y., et al.** (1998). Cellular and developmental control of O2
512 homeostasis by hypoxia-inducible factor 1 alpha. *Genes & development* **12**, 149-162.
513 **Lan, W. and Cleveland, D. W.** (2010). A chemical tool box defines mitotic and interphase roles for Mps1
514 kinase. *The Journal of cell biology* **190**, 21-24.
515 **Lee, K. and Kim, H. M.** (2011). A novel approach to cancer therapy using PX-478 as a HIF-1alpha
516 inhibitor. *Arch Pharm Res* **34**, 1583-1585.
517 **Marti, J. M., Garcia-Diaz, A., Delgado-Bellido, D., O'Valle, F., Gonzalez-Flores, A., Carlevaris, O.,**
518 **Rodriguez-Vargas, J. M., Ame, J. C., Dantzer, F., King, G. L., et al.** (2021). Selective
519 modulation by PARP-1 of HIF-1alpha-recruitment to chromatin during hypoxia is required for
520 tumor adaptation to hypoxic conditions. *Redox Biol* **41**, 101885.
521 **McCoy, R. C.** (2017). Mosaicism in Preimplantation Human Embryos: When Chromosomal Abnormalities
522 Are the Norm. *Trends Genet* **33**, 448-463.
523 **Meuter, A., Rogmann, L. M., Winterhoff, B. J., Tchkonia, T., Kirkland, J. L. and Morbeck, D. E.**
524 (2014). Markers of cellular senescence are elevated in murine blastocysts cultured in vitro:
525 molecular consequences of culture in atmospheric oxygen. *J Assist Reprod Genet* **31**, 1259-
526 1267.
527 **Mole, M. A., Weberling, A. and Zernicka-Goetz, M.** (2020). Comparative analysis of human and mouse
528 development: From zygote to pre-gastrulation. *Current topics in developmental biology* **136**, 113-
529 138.
530 **Muzumdar, M. D., Tasic, B., Miyamichi, K., Li, L. and Luo, L.** (2007). A global double-fluorescent Cre
531 reporter mouse. *Genesis* **45**, 593-605.
532 **Nakamura, H., Sekine, H., Kato, H., Masai, H., Gradin, K. and Poellinger, L.** (2022). Hypoxia-inducible
533 factor-1alpha and poly [ADP ribose] polymerase 1 cooperatively regulate Notch3 expression
534 under hypoxia via a noncanonical mechanism. *J Biol Chem* **298**, 102137.
535 **Nguyen, A. Q., Bardua, I., Greene, B., Wrenzycki, C., Wagner, U. and Ziller, V.** (2020). Mouse
536 embryos exposed to oxygen concentrations that mimic changes in the oviduct and uterus show
537 improvement in blastocyst rate, blastocyst size, and accelerated cell division. *Reprod Biol* **20**,
538 147-153.
539 **Palmerola, K. L., Amrane, S., De Los Angeles, A., Xu, S., Wang, N., de Pinho, J., Zuccaro, M. V.,**
540 **Taglialatela, A., Massey, D. J., Turocy, J., et al.** (2022). Replication stress impairs chromosome
541 segregation and preimplantation development in human embryos. *Cell* **185**, 2988-3007 e2920.
542 **Pauerova, T., Radonova, L., Kovacovicova, K., Novakova, L., Skultety, M. and Anger, M.** (2020).
543 Aneuploidy during the onset of mouse embryo development. *Reproduction* **160**, 773-782.

544 **Pietrzak, J., Spickett, C. M., Ploszaj, T., Virag, L. and Robaszkiewicz, A.** (2018). PARP1 promoter
545 links cell cycle progression with adaptation to oxidative environment. *Redox Biol* **18**, 1-5.
546 **Santaguida, S., Tighe, A., D'Alise, A. M., Taylor, S. S. and Musacchio, A.** (2010). Dissecting the role
547 of MPS1 in chromosome biorientation and the spindle checkpoint through the small molecule
548 inhibitor reversine. *The Journal of cell biology* **190**, 73-87.
549 **Shahbazi, M. N., Wang, T., Tao, X., Weatherbee, B. A. T., Sun, L., Zhan, Y., Keller, L., Smith, G. D.,**
550 **Pellicer, A., Scott, R. T., Jr., et al.** (2020). Developmental potential of aneuploid human embryos
551 cultured beyond implantation. *Nature communications* **11**, 3987.
552 **Simoes-Sousa, S., Littler, S., Thompson, S. L., Minshall, P., Whalley, H., Bakker, B., Belkot, K.,**
553 **Moralli, D., Bronder, D., Tighe, A., et al.** (2018). The p38alpha Stress Kinase Suppresses
554 Aneuploidy Tolerance by Inhibiting Hif-1alpha. *Cell reports* **25**, 749-760 e746.
555 **Singla, S., Iwamoto-Stohl, L. K., Zhu, M. and Zernicka-Goetz, M.** (2020). Autophagy-mediated
556 apoptosis eliminates aneuploid cells in a mouse model of chromosome mosaicism. *Nature*
557 *communications* **11**, 2958.
558 **Soto, M., Raaijmakers, J. A., Bakker, B., Spierings, D. C. J., Lansdorp, P. M., Foijer, F. and**
559 **Medema, R. H.** (2017). p53 Prohibits Propagation of Chromosome Segregation Errors that
560 Produce Structural Aneuploidies. *Cell reports* **19**, 2423-2431.
561 **Starostik, M. R., Sosina, O. A. and McCoy, R. C.** (2020). Single-cell analysis of human embryos reveals
562 diverse patterns of aneuploidy and mosaicism. *Genome Res* **30**, 814-825.
563 **Thompson, S. L. and Compton, D. A.** (2010). Proliferation of aneuploid human cells is limited by a p53-
564 dependent mechanism. *The Journal of cell biology* **188**, 369-381.
565 **Vanneste, E., Voet, T., Le Caignec, C., Ampe, M., Konings, P., Melotte, C., Debrock, S., Amyere, M.,**
566 **Vikkula, M., Schuit, F., et al.** (2009). Chromosome instability is common in human cleavage-
567 stage embryos. *Nature medicine* **15**, 577-583.
568 **Vazquez-Diez, C., Paim, L. M. G. and FitzHarris, G.** (2019). Cell-Size-Independent Spindle Checkpoint
569 Failure Underlies Chromosome Segregation Error in Mouse Embryos. *Current biology : CB* **29**,
570 865-873 e863.
571 **Zhao, T., Ren, H., Jia, L., Chen, J., Xin, W., Yan, F., Li, J., Wang, X., Gao, S., Qian, D., et al.** (2015).
572 Inhibition of HIF-1alpha by PX-478 enhances the anti-tumor effect of gemcitabine by inducing
573 immunogenic cell death in pancreatic ductal adenocarcinoma. *Oncotarget* **6**, 2250-2262.
574 **Zhu, J., Tsai, H. J., Gordon, M. R. and Li, R.** (2018). Cellular Stress Associated with Aneuploidy.
575 *Developmental cell* **44**, 420-431.
576 **Zhu, M., Shahbazi, M., Martin, A., Zhang, C., Sozen, B., Borsos, M., Mandelbaum, R. S., Paulson, R.**
577 **J., Mole, M. A., Esbert, M., et al.** (2021). Human embryo polarization requires PLC signaling to
578 mediate trophectoderm specification. *Elife* **10**.
579 **Zhu, M. and Zernicka-Goetz, M.** (2020). Principles of Self-Organization of the Mammalian Embryo. *Cell*
580 **183**, 1467-1478.
581

582 **FIGURES AND FIGURE LEGENDS**

583 Figure 1| **Lineage analysis of aneuploid embryos generated by selective Mps1 inhibitors AZ3146 and**
584 **reversine.**

585 (A) Graphic representation of 4-cell embryos treated with DMSO (control) or Mps1 inhibitors reversine (0.5
586 μM) and AZ3146 (20 μM) to inactivate the spindle assembly checkpoint (SAC) and induce chromosome
587 segregation errors. After washing, embryos were cultured to the mature blastocyst stage (E4.5) and
588 analyzed for lineage specification. (B) Immunofluorescence imaging of well-known lineage markers CDX2
589 (TE), NANOG (EPI) and SOX17 (PE) reveals that overall embryonic morphology and cavitation is not
590 affected by Mps1 inhibition. (C) Number of cells in each lineage was quantified to evaluate the effect of
591 drug treatment on blastocyst development. Importantly, both reversine and AZ3146-treatments reduce the
592 number of cells in the ICM, marked by NANOG (EPI) and SOX17 (PE). Whereas the TE, marked by CDX2,
593 is reduced only in the reversine-treated embryos. (n=28 per treatment) (***P<0.0001, **P<0.01, *P<0.05,

594 Mann–Whitney U-test, error bars represent s.e.m). (D) Analysis of DNA damage and DNA repair based on
595 immunofluorescence against γH2A.X (phosphorylated form of H2A.X, white) and PARP1 (red),
596 respectively. (E) Intensity analysis shows that reversine and AZ3146 increase DNA damage at the 8-cell
597 stage through morula stage. Importantly, reversine appears to downregulate PARP1 expression at the 8-
598 cell stage, which extends to morula stage embryos (***P<0.0001, **P<0.01, *P<0.05, t-test).
599
600 Figure 2 | **AZ3146-treated embryos elevate HIF1A activity to support formation of the TE and PE.**
601 A) qPCR analysis of *p53* and *Hif1a* mRNA expression at morula and blastocyst stages reveals that *p53* is
602 upregulated in reversine-treated embryos and that *Hif1a* is upregulated in AZ3146-treated embryos at
603 morula stages; 3 biological replicates and 2 technical replicates per experiment with each replicate having
604 a minimum of 16 embryos (**P<0.01, *P<0.05, Welch's t-test). B) Immunofluorescence against HIF1A
605 (black) shows an increase in nuclear intensity in AZ3146-treated embryos at morula stages. At blastocyst
606 stage, nuclear and cytoplasmic HIF1A are increased in AZ3146-treated embryos; normalization was based
607 on DAPI staining (magenta). (C) Graphic representation of 4-cell embryos treated with DMSO and
608 aneuploid drugs. Chemical downregulation of HIF1A was achieved by treatment with IDF-11774
609 immediately after wash of the aneuploid drugs. Immunofluorescence analysis of lineage specification in
610 blastocyst cultured with the HIF1A inhibitor IDF-11774 using antibodies against CDX2 (TE), NANOG (EPI)
611 and SOX17 (PE). Importantly, IDF-11774 appears to affect cavitation of some AZ3146-treated embryos.
612 (D) Lineage analysis at the blastocyst stage shows that TE and PE specification are affected by IDF-11774
613 treatment. Number of cells in each lineage was quantified to evaluate the effect in blastocyst development.
614 (***P<0.0001, **P<0.01, *P<0.05, Mann–Whitney U-test, error bars represent s.e.m).
615
616 Figure 3 | **Hypoxia exposure reduces DNA damage and affects lineage proportions in the aneuploid**
617 **blastocyst.**
618 (A) Graphic representation of the hypoxia experiments. 2-cell embryos were cultured until the blastocyst
619 stage in hypoxia conditions (5% oxygen). As before, 4-cell stage embryos were treated with DMSO or Mps1
620 inhibitors reversine and AZ3146 until the 8-cell stage. After washing, embryos were cultured to the mature
621 blastocyst stage (E4.5) and analyzed for lineage specification. (B) Immunofluorescence imaging of well-
622 known lineage markers CDX2 (TE), NANOG (EPI) and SOX17 (PE) reveals that overall embryonic
623 morphology and cavitation is not affected by Mps1 inhibition or hypoxia. (C) Lineage analysis at blastocyst
624 stage. Number of cells in each lineage was used to evaluate the effects in blastocyst development.
625 (*P<0.05, Mann–Whitney U-test, error bars represent s.e.m). (D) Immunofluorescence against PARP1 (red)
626 and γH2A.X (white) in blastocyst after drug treatments. (E) Intensity analysis shows that, under hypoxia,
627 DNA damage is only slightly increased at the 8-cell stage after exposure to reversine and AZ3146. PARP1
628 expression is altered only at the 8-cell stage in reversine-treated embryos (***P<0.0001, **P<0.01, *P<0.05,
629 t-test).
630

631 Figure 4 | **Hypoxia affects cell competition between diploid and aneuploid cells during pre-**
632 **implantation development.** (A) Graphic representation of the cell competition experiments. Embryos were
633 treated at the 4-cell stage with DMSO or Mps1 inhibitors reversine and AZ3146. After washing, 8-cell stage
634 embryos were disaggregated, and re-aggregated to form chimeras containing a 1:1 ratio of DMSO/AZ314-
635 treated blastomeres and reversine/DMSO-treated blastomeres. Following aggregation, chimeras were
636 cultured to the mature blastocyst stage (E4.5) and analyzed for lineage specification. For identification of
637 the treatment, we use transgenics lines with membrane markers. Immunofluorescence for CDX2, NANOG,
638 and SOX17 was performed to test lineage specification and allocation during (B) normoxia and (C) hypoxia.
639 Lineage allocation quantification was based on the above markers. Importantly, D) in normoxia, both
640 chimeras have the same number of cells in all the lineages except the EPI. In addition, AZ3146-treated
641 blastomeres outcompete reversine-treated blastomeres in medium-grade mosaics in the TE and the EPI.
642 E) Under hypoxia, both chimeras have similar number of cells in all the lineages. Yet, AZ3146-blastomeres
643 do not outcompete reversine-treated blastomeres. Quantification of the contribution of AZ3146-treated
644 blastomeres to the chimeras showed that, (F) under normoxia, compare with DMSO-treated cells, no
645 preferential allocation of aneuploid cells occurs in the TE. In contrast, AZ3146-treated blastomeres
646 increased their contribution when compare with reversine- treated blastomeres, but only significantly on the
647 EPI and the PE. (G) During hypoxia, DMSO/AZ3146 chimeras did not change their behavior. Confirming a
648 preferential allocation of diploid cells to the EPI. In reversine/AZ3146 chimeras, AZ3146-treated
649 blastomeres contribute similarly to reversine-blastomeres to the TE and EPI but significantly increase
650 contribution to the EPI. These results indicate that hypoxia favors the survival of reversine-induced
651 aneuploid cells (Experiments were repeated in triplicate, ****P<0.00001, **P<0.01, *P<0.05, Mann–Whitney
652 U-test, error bars represent s.e.m).
653
654 Figure 5| **HIF1A inhibition increases the proportion of euploid cells in mosaic embryos.** (A) Schematic
655 of HIF1A inhibition by IDF-11774 in 8-cell stage aggregation chimeras cultured in hypoxia.
656 Immunofluorescence for CDX2, NANOG, and SOX17 was performed to test lineage specification and
657 allocation. (B) HIF1A inhibition in low-grade mosaicism does not affect overall morphology but affects (C)
658 cavitation. In contrast, (E) HIF1A inhibition in medium-grade mosaicism affects morphology, and (F)
659 cavitation of the embryos. Lineage allocation quantification after IDF-1174 reveals a significant reduction
660 of total cell number (D) in low-grade mosaicism as well as a reduction in cell number in the TE but not in
661 the EPI and PE. In contrast, total cell number is not affected (G) in medium-grade mosaicism. However,
662 IDF11-774 treatment appears to increase the cell number of the PE. These results show that HIF1A
663 inhibition in hypoxic conditions differentially affect each type of mosaic embryos. Experiments were
664 repeated in triplicate, **P<0.005, *P<0.05, Mann–Whitney U-test, error bars represent s.e.m.
665
666 Figure S.1| **AZ3146-treated embryos are aneuploid and can develop to post-implantation stages.**

667 (A) *In situ* chromosome counting of 8-cell stage embryos after drug treatments. Representative images of
668 individual embryos in the different treatments. DNA (white) is visualized by DAPI staining and kinetochores
669 (red) by CREST antibody. PB (polar body), MN (micronuclei). Each chromosome presents 2 CREST dots.
670 The large number is the cell ID and the smaller number indicates the number of chromosomes, "n". Diploid
671 blastomeres present 40 pairs of CREST dots. Phalloidin (cyan) was used for cell segmentation. (B)
672 Quantification of the incidence of aneuploid events, designated as those with more than 2 chromosomes
673 (MN>2chr), less than 2 chromosomes (MN<2chr), without kinetochores (MN-CREST) and non-dividing
674 nucleus (ND cell). We observed an increase in MN following reversine and AZ3146 treatment. Importantly,
675 reversine-treated cells have a higher number of ND cells and MN-CREST staining. (n=128 cell DMSO
676 treatment, n=152 cells AZ3146 treatment, n=72 cells reversine treatment, ****P<0.00001, **P<0.01,
677 *P<0.05, Mann–Whitney U-test, error bars represent s.e.m). (C) Embryo transfer experiments show higher
678 implantation events (% decidua formation) in AZ3146-treated embryos. The left uterine horn was used for
679 transfer of reversine-treated blastocyst and the right uterine horn for AZ3146-treated blastocyst. (D) Only
680 AZ3146-treated blastocyst can develop post-gastrulation E9.5 fetuses (% embryo formation).
681
682 Figure S.2| **PARP1 is required for ICM development**.
683 (A) Immunofluorescence against PARP1 (red) and γH2A.X (white) in blastocyst after drug treatments.
684 Notice accumulation of DNA damage in reversine-treated blastocyst. (B) Immunofluorescence against
685 PARP1 (red), NANOG (white, epiblast) and CDX2 (green, trophectoderm). Analysis of PARP1 intensity
686 shows an increase in the EPI lineage. To confirm these observation, scRNA-seq (Deng et. al 2014) shows
687 enrichment of *Parp1* mRNA specifically in the EPI. (C) Graphic representation of 4-cell embryos treated
688 with DMSO and aneuploid drugs. Chemical downregulation of PARP1 was achieved by treatment with
689 Olaparib from morula to blastocyst stage. (D) Effects of the inhibition of PARP1 function were assessed by
690 immunofluorescence against CDX2 (TE), NANOG (EPI) and SOX17 (PE) in the different treatments.
691 Importantly, Olaparib treatment does not affect blastocyst morphology. (E) Lineage analysis at blastocyst
692 stage shows a specific effect on the survival of epiblast and PE cells in reversine-treated embryos. Ratio of
693 cells in each lineage in the blastocyst is normalized based on DMSO treatment. (***P<0.0001, **P<0.01,
694 *P<0.05, Mann–Whitney U-test, error bars represent s.e.m).
695
696 Figure S.3| **Pharmacological inhibitors of HIF1A have distinct effects on mouse pre-implantation**
697 **embryos.** (A) Chemical inhibition of HIF1A from zygotes to blastocyst stage with PX-478 or IDF-11774.
698 Immunofluorescence against CDX2 (TE) and DAPI (magenta) was used to assess blastocyst development.
699 Importantly, IDF-11774 does not compromise pre-implantation development, whereas PX-478
700 compromised the survival and overall morphology of the blastocyst. (B) Analysis of the number of
701 trophectoderm cells (CDX2) and total number (DAPI) shows a deleterious effect of PX-478 during blastocyst
702 development (***P<0.0001, **P<0.01, *P<0.05, Mann–Whitney U-test, error bars represent s.e.m).
703

704 Figure S.4| **Correlation plot of AZ3146-treated cells in the epiblast and trophectoderm.** Scatter plot of
705 AZ3146-treated cells in epiblast and trophectoderm in DMSO/AZ3146 mosaic blastocysts.
706
707 Figure S.5| **Aneuploidies generated at different stages have similar consequences on post-**
708 **implantation development *in vitro*.** (A) Immunofluorescence for CDX2, NANOG, and SOX17 was
709 performed in blastocysts after zygote treatment with Mps1 inhibitors. Importantly, reversine treatment at
710 zygote stages affects morphology of blastocyst. (B) Lineage analysis of blastocyst shows no effect in
711 AZ3146-treated embryos. Whereas reversine treatment reduces the cell number to almost half. Ratio of
712 cells in each lineage in the blastocyst is normalized based on DMSO treatments. (n>27 per treatment)
713 (***P<0.0001, **P<0.01, *P<0.05, Mann–Whitney U-test, error bars represent s.e.m). (C) Aggregation
714 chimeras at 2-cell stage were created by using transgenics lines with membrane markers: mTmG (green)
715 and E-cadherin (white). Subsequently, (D) immunofluorescence for CDX2, NANOG, and SOX17 was
716 performed to quantify lineage allocation. Our results show no effect on embryo morphology in our chimeras.
717 However, reversine/DMSO (D/R) chimeras seems to have increase events of cell extrusion and
718 reversine/AZ3146 chimeras are smaller in number of cells compare with DMSO/AZ3146 chimeras. (E) Data
719 show the proportion of AZ3146-treated cells in DMSO/AZ3146 mosaic blastocysts (grey) and in
720 reversine/AZ3146 mosaic blastocysts (blue), as well as the proportion of reversine-treated cells in
721 DMSO/reversine mosaic blastocysts (red).
722
723 Figure S.6| **IDF-11774-mediated inhibition of HIF1A increases the proportion of euploid cells in**
724 **mosaic embryos.** Brightfield images of low- and medium-grade chimeras grown in (A) DMSO and (B) IDF-
725 11774. Quantification of the contribution of AZ3146-treated blastomeres to the chimeras showed that, (C)
726 in DMSO/AZ3146 mosaics, IDF-11774 treatment reduces the proportion of AZ3146-treated blastomeres,
727 whereas (D) in reversine/AZ3146 mosaics, IDF-11774 treatment slightly increases the proportion of
728 AZ3146-treated blastomeres. These results may indicate that HIF1A inhibition impairs the less fit population
729 in chimeric embryos.
730

Figure 1

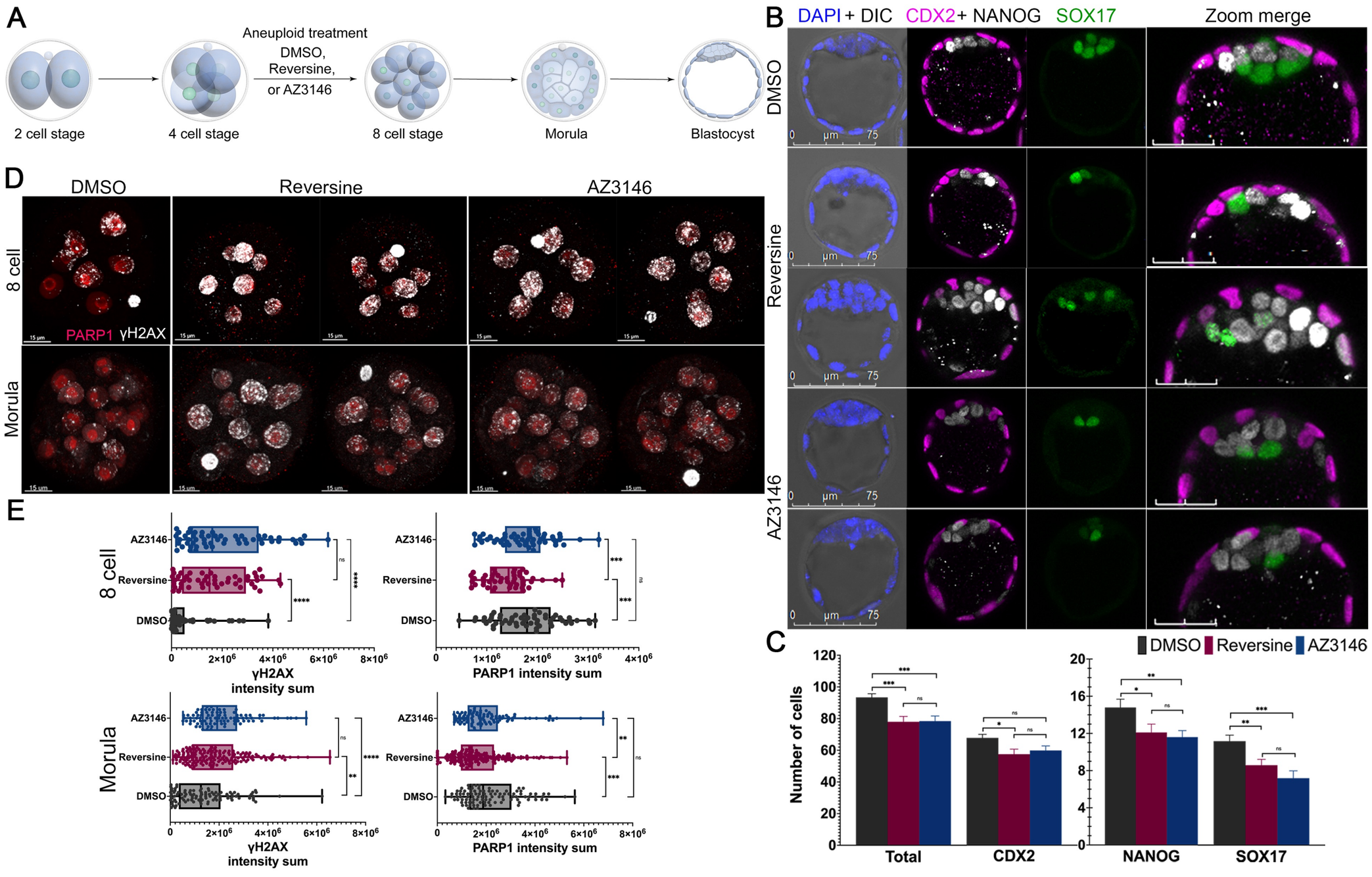
A
Aneuploid treatment
DMSO,
Reversine,
or AZ3146
2 cell stage
4 cell stage
8 cell stage
Morula
Blastocyst
B
DAPI + DIC
CDX2+ NANOG
SOX17
Zoom merge
DMSO
Reversine
AZ3146
C
DMSO
Reversine
AZ3146
Number of cells
Total
CDX2
NANOG
SOX17
D
DMSO
Reversine
AZ3146
8 cell
Morula
PARP1
γH2AX
E
8 cell
Morula
AZ3146
Reversine
DMSO
γH2AX
intensity sum
PARP1 intensity sum

Figure 2

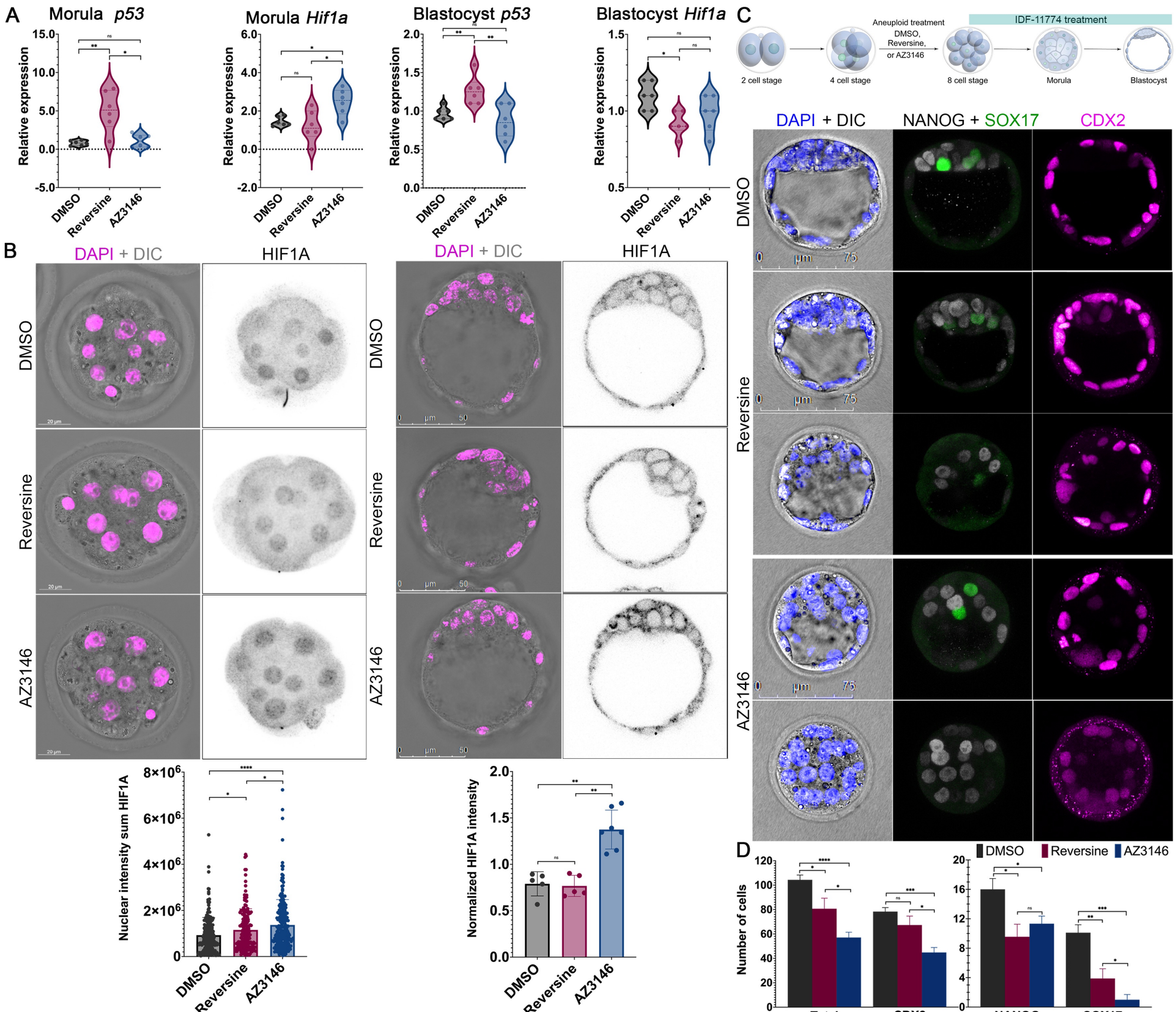
A
Morula p53
Morula Hif1a
Blastocyst p53
Blastocyst Hif1a
Relative expression
DMSO
Reversine
AZ3146
B
DAPI + DIC
HIF1A
DMSO
Reversine
AZ3146
Nuclear intensity sum HIF1A
Normalized HIF1A intensity
C
Aneuploid treatment
DMSO, Reversine, or AZ3146
IDF-11774 treatment
2 cell stage
4 cell stage
8 cell stage
Morula
Blastocyst
DAPI + DIC
NANOG + SOX17
CDX2
D
DMSO
Reversine
AZ3146
Number of cells
Total
CDX2
NANOG
SOX17

Figure 3

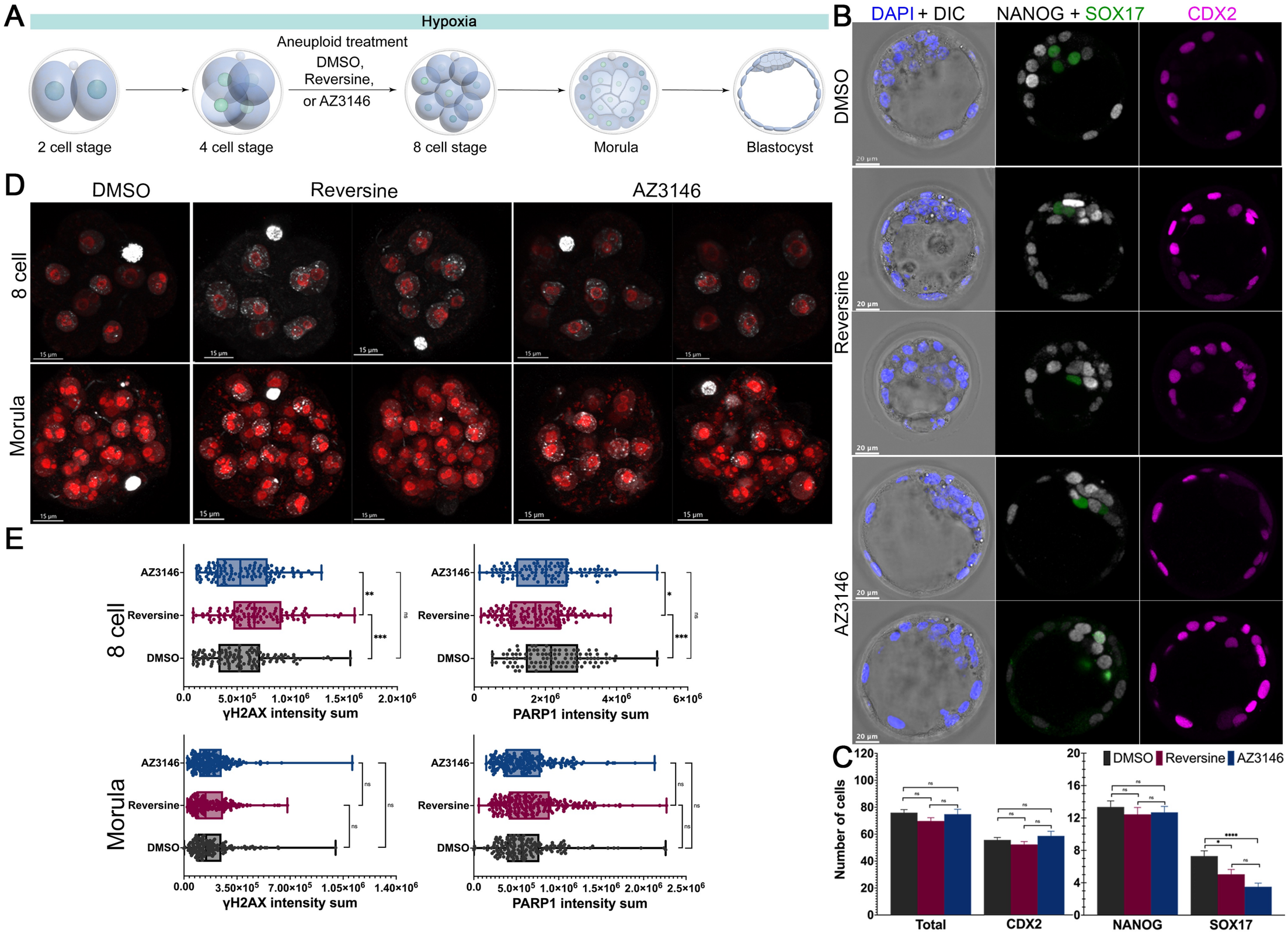
A
Hypoxia
Aneuploid treatment
DMSO,
Reversine,
or AZ3146
2 cell stage
4 cell stage
8 cell stage
Morula
Blastocyst
B
DAPI + DIC
NANOG + SOX17
CDX2
DMSO
Reversine
AZ3146
20 µm
C
DMSO
Reversine
AZ3146
Number of cells
Total
CDX2
NANOG
SOX17
D
DMSO
Reversine
AZ3146
8 cell
Morula
15 µm
E
8 cell
Morula
AZ3146
Reversine
DMSO
γH2AX intensity sum
PARP1 intensity sum
ns

Figure 4

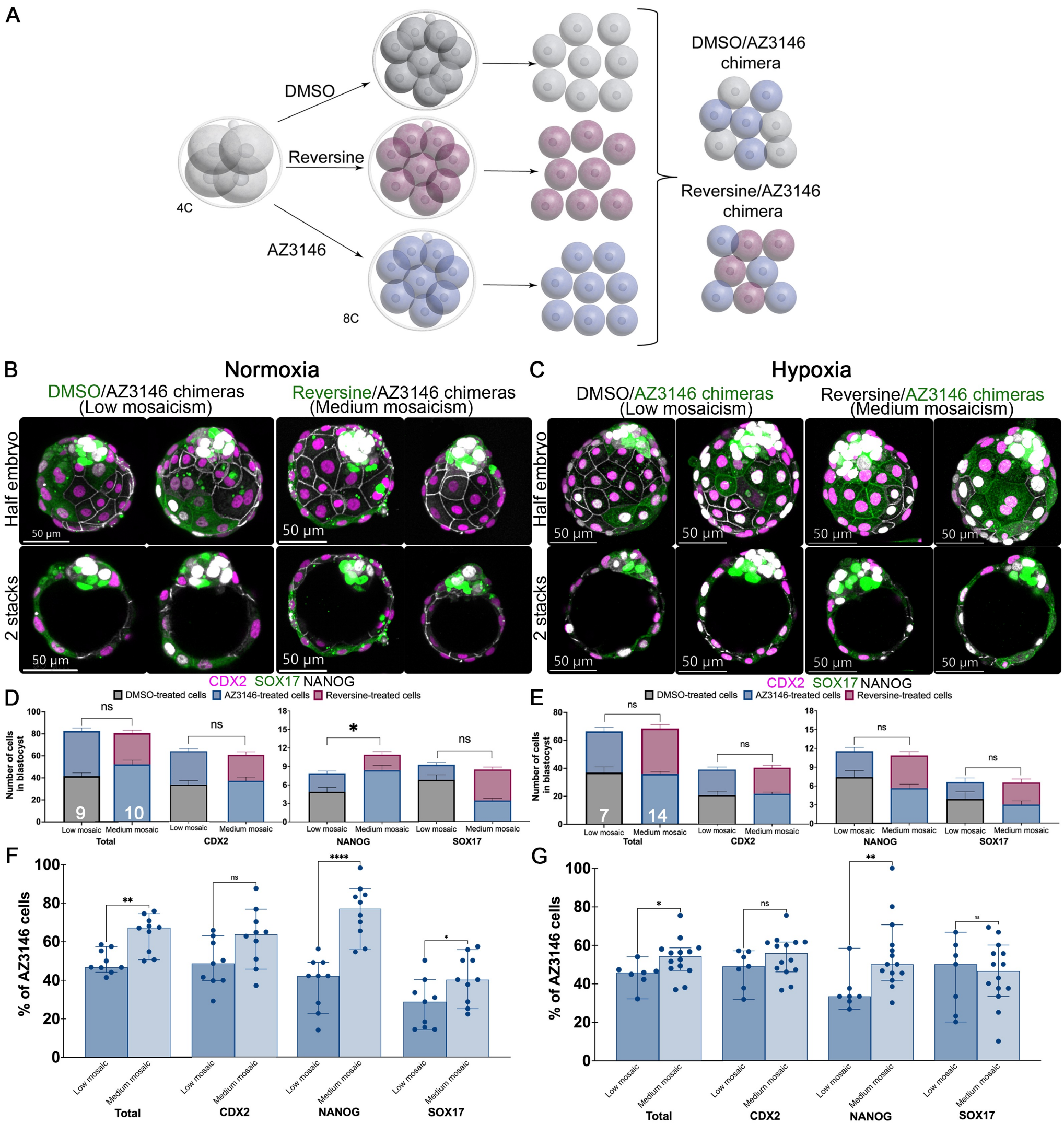
A
DMSO
Reversine
AZ3146
4C
8C
DMSO/AZ3146 chimera
Reversine/AZ3146 chimera
B
Normoxia
DMSO/AZ3146 chimeras (Low mosaicism)
Reversine/AZ3146 chimeras (Medium mosaicism)
Half embryo
2 stacks
50 µm
C
Hypoxia
DMSO/AZ3146 chimeras (Low mosaicism)
Reversine/AZ3146 chimeras (Medium mosaicism)
CDX2 SOX17 NANOG
D
DMSO-treated cells
AZ3146-treated cells
Reversine-treated cells
Number of cells in blastocyst
ns
*
9
10
Low mosaic
Medium mosaic
Total
CDX2
NANOG
SOX17
E
7
14
F
% of AZ3146 cells
**
****
G

Figure 5

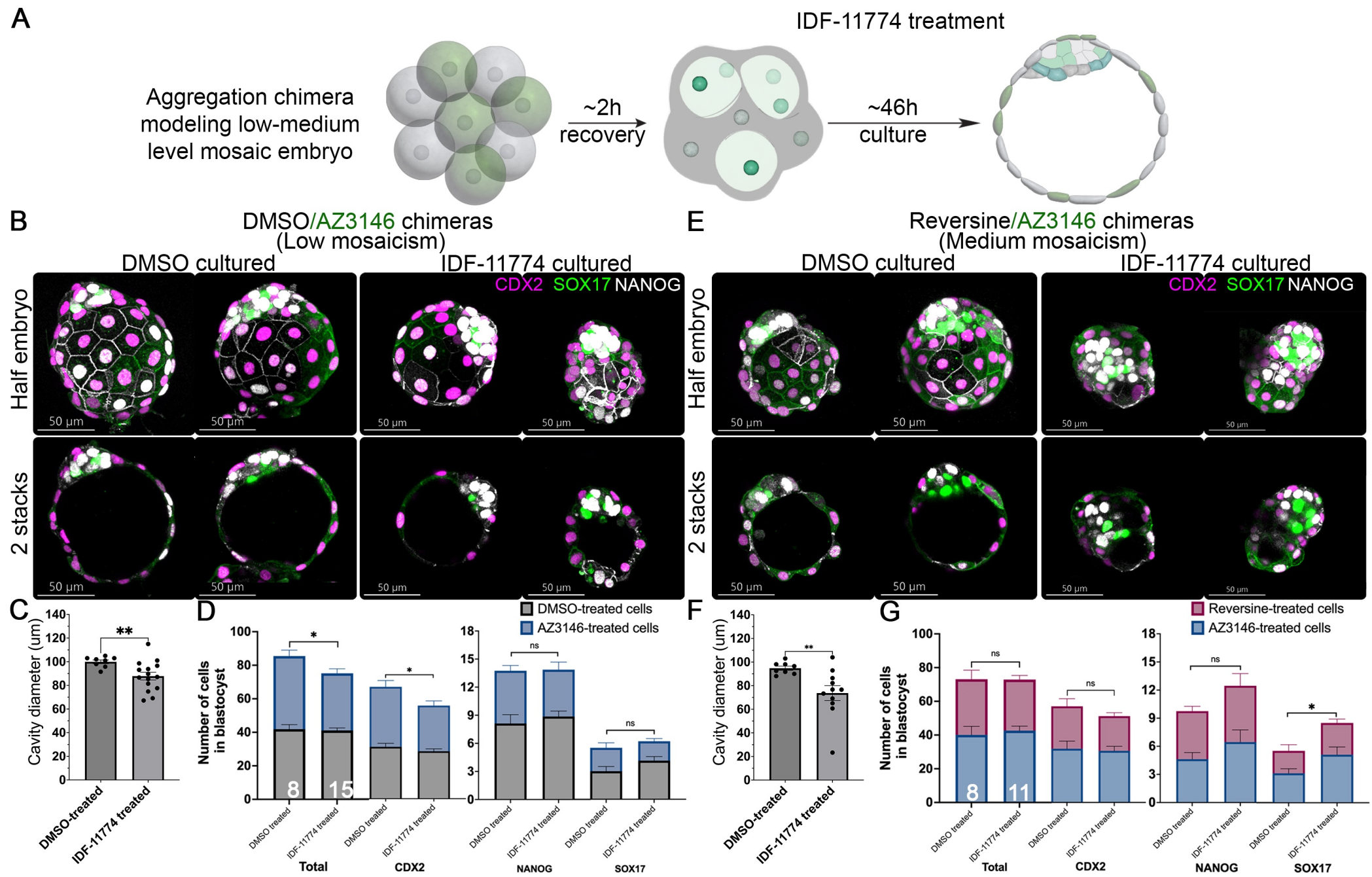
A
IDF-11774 treatment
Aggregation chimera modeling low-medium level mosaic embryo
~2h recovery
~46h culture
B
DMSO/AZ3146 chimeras (Low mosaicism)
DMSO cultured
IDF-11774 cultured
CDX2 SOX17 NANOG
Half embryo
2 stacks
50 µm
E
Reversine/AZ3146 chimeras (Medium mosaicism)
C
Cavity diameter (um)
DMSO-treated
IDF-11774 treated
D
Number of cells in blastocyst
DMSO-treated cells
AZ3146-treated cells
Total
CDX2
NANOG
SOX17
F
G
Reversine-treated cells

Figure S. 1

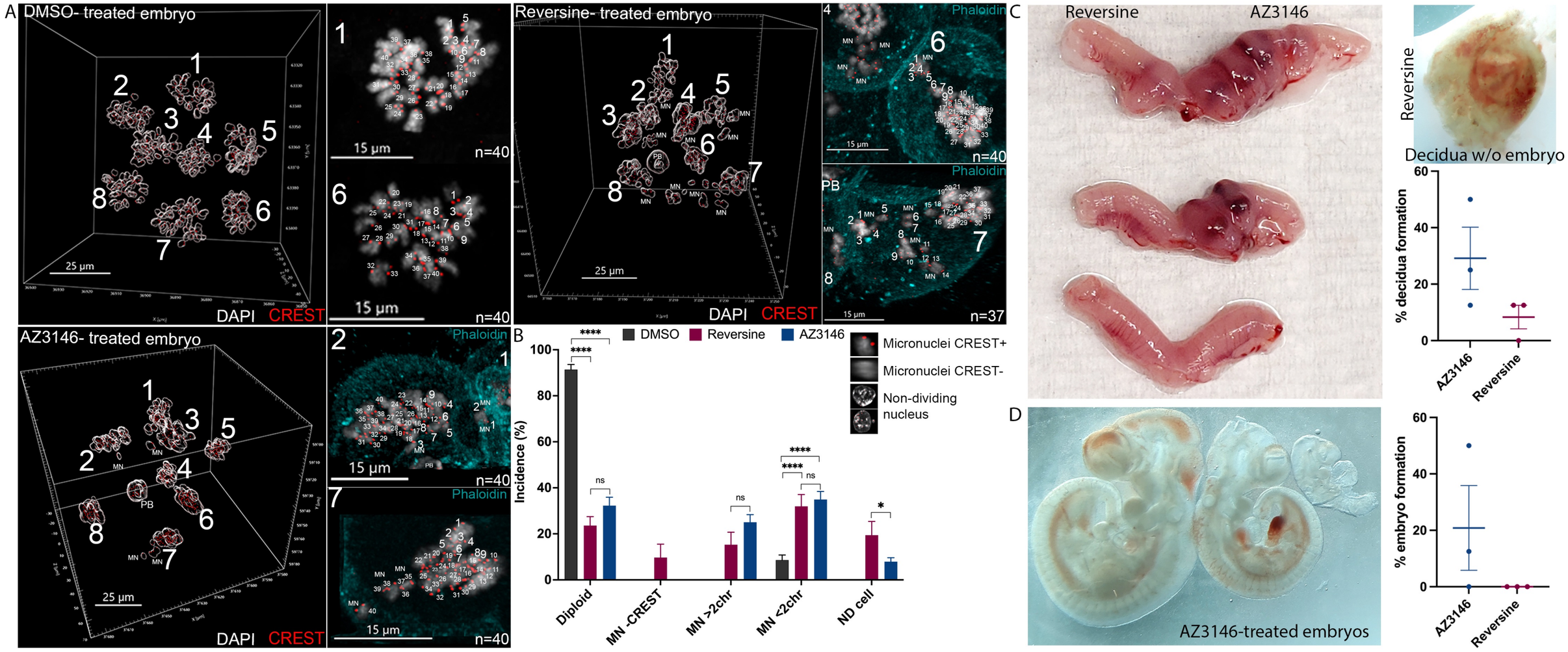
A
DMSO- treated embryo
25 µm
DAPI CREST
15 µm
n=40
Reversine- treated embryo
Phaloidin
n=37
AZ3146- treated embryo
B
DMSO
Reversine
AZ3146
Micronuclei CREST+
Micronuclei CREST-
Non-dividing nucleus
Incidence (%)
Diploid
MN -CREST
MN >2chr
MN <2chr
ND cell
C
Reversine
AZ3146
Decidua w/o embryo
% decidua formation
D
AZ3146-treated embryos
% embryo formation

Figure S.2

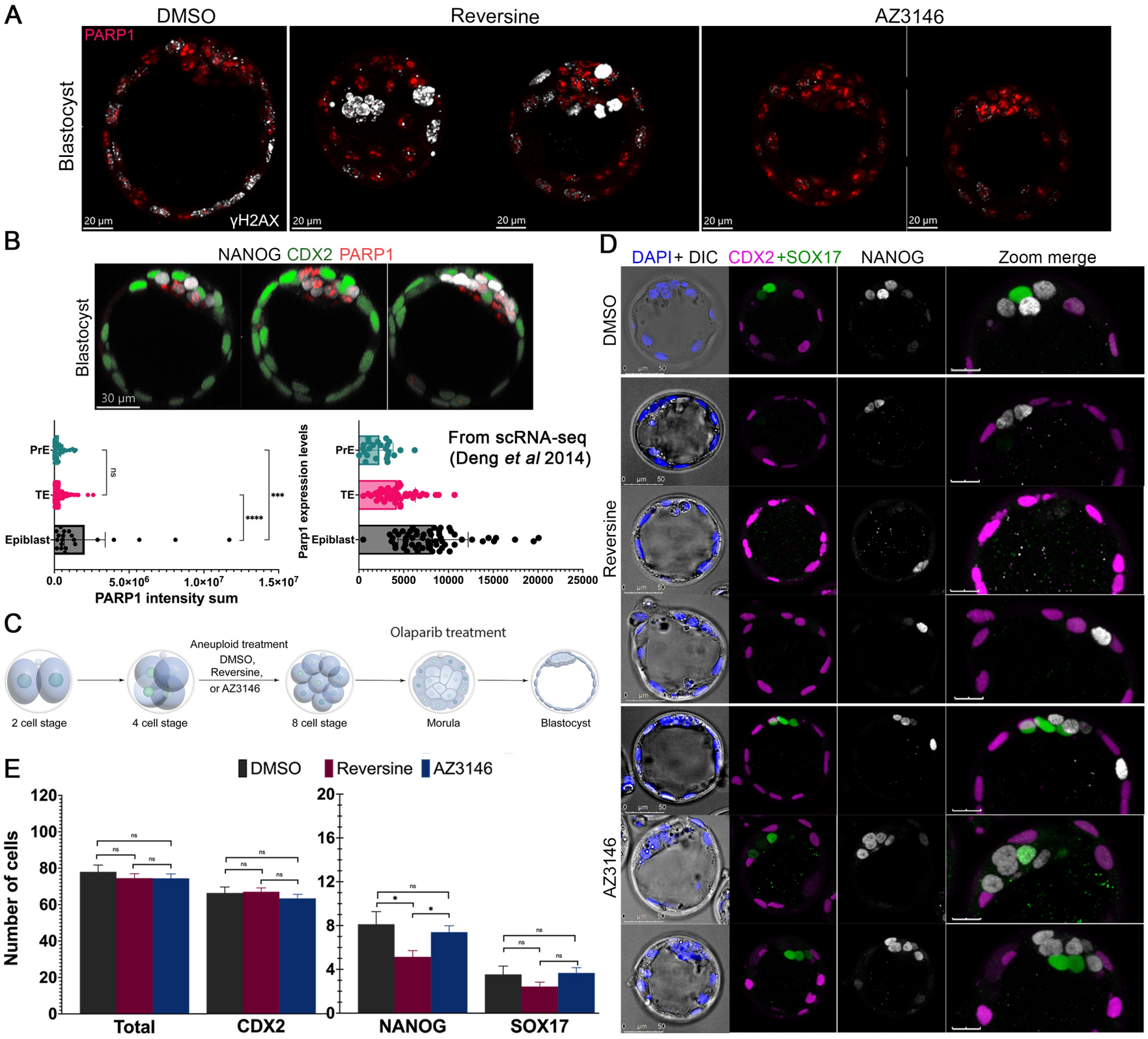
A
DMSO
Reversine
AZ3146
PARP1
Blastocyst
γH2AX
20 µm
B
NANOG CDX2 PARP1
Blastocyst
30 µm
PrE
TE
Epiblast
ns
***
****
0.0
5.0×10^6
1.0×10^7
1.5×10^7
PARP1 intensity sum
Parp1 expression levels
From scRNA-seq
(Deng et al 2014)
0
5000
10000
15000
20000
25000
C
Aneuploid treatment
DMSO,
Reversine,
or AZ3146
Olaparib treatment
2 cell stage
4 cell stage
8 cell stage
Morula
Blastocyst
D
DAPI + DIC
CDX2 +SOX17
NANOG
Zoom merge
DMSO
Reversine
AZ3146
E
DMSO
Reversine
AZ3146
Number of cells
Total
CDX2
NANOG
SOX17
ns
*

Figure S. 3

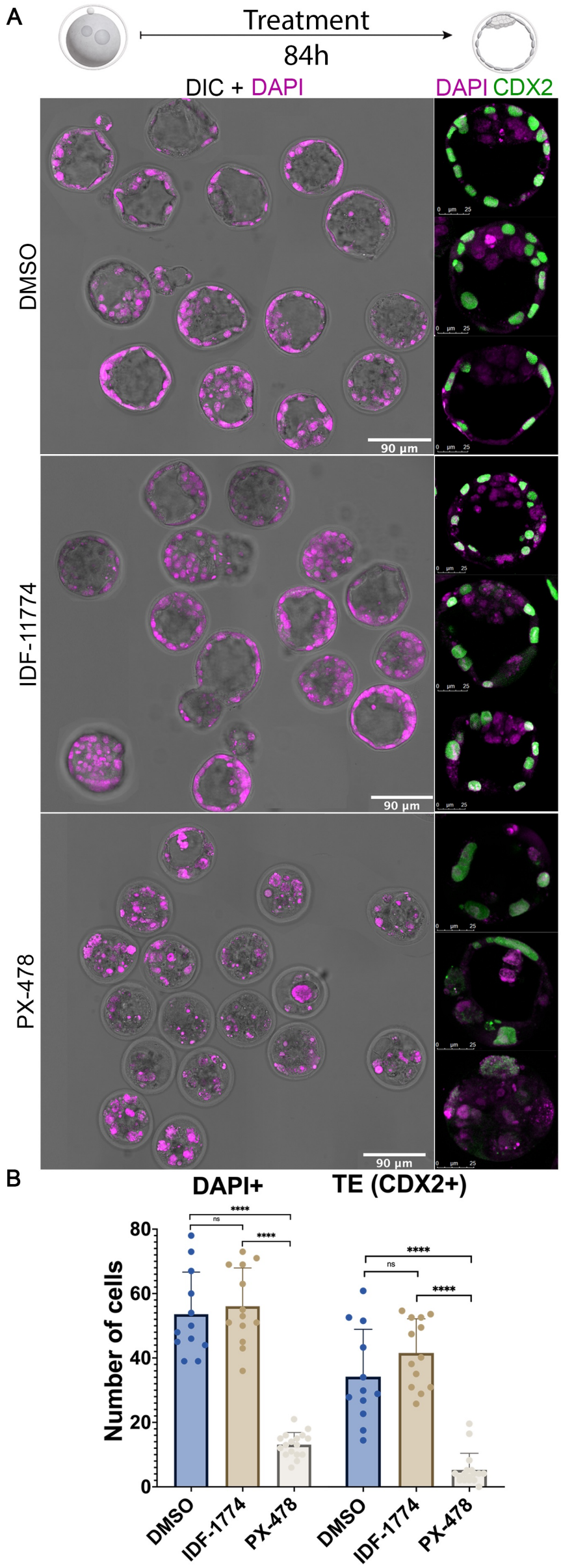
A
Treatment
84h
DIC + DAPI
DAPI CDX2
DMSO
IDF-11774
PX-478
90 µm
B
DAPI+
TE (CDX2+)
Number of cells
80
60
40
20
0
****
ns
DMSO
IDF-1774
PX-478

Figure S. 4

A

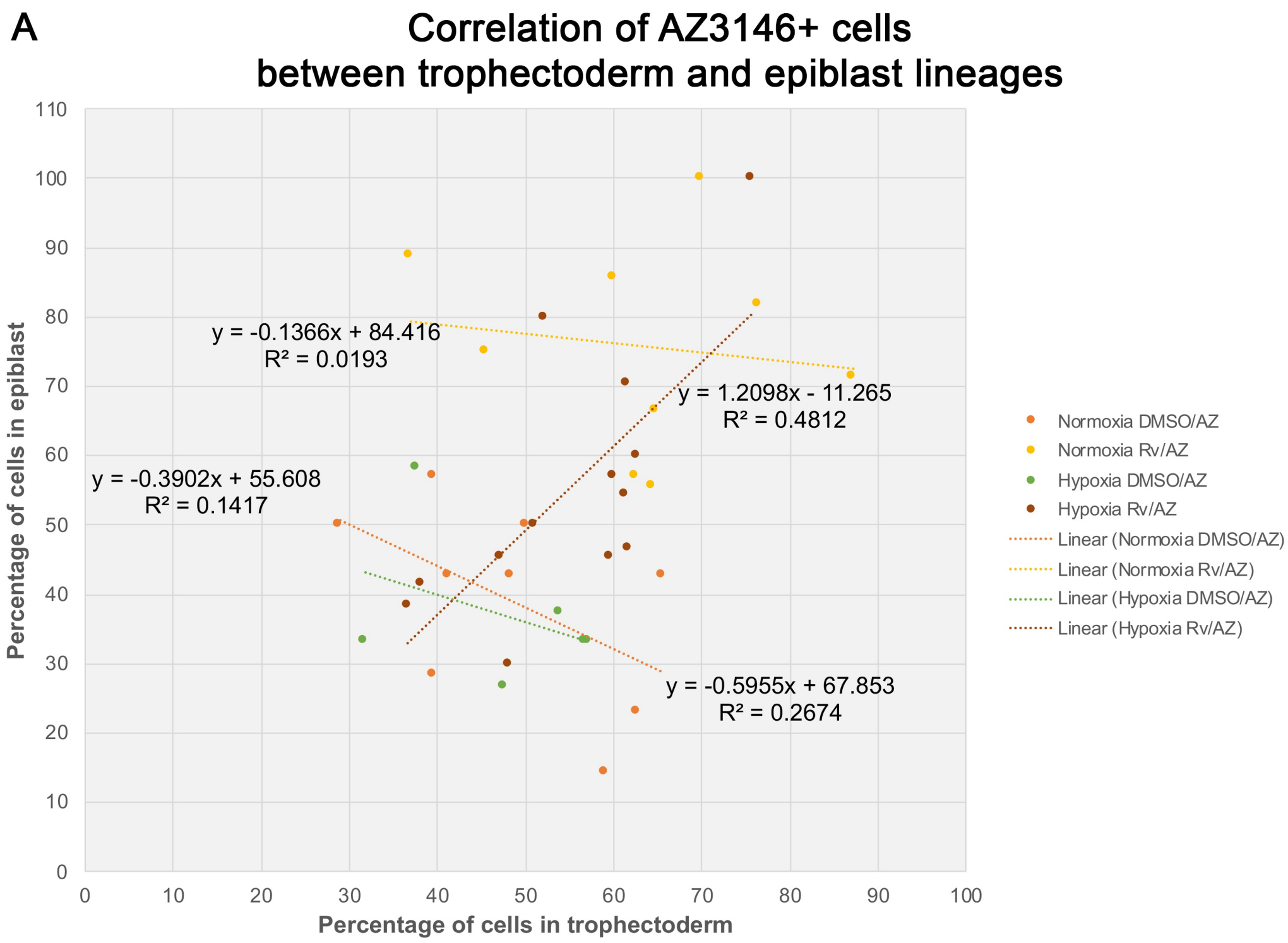
Correlation of AZ3146+ cells
between trophectoderm and epiblast lineages
Percentage of cells in epiblast
Percentage of cells in trophectoderm
0
10
20
30
40
50
60
70
80
90
100
110
y = -0.1366x + 84.416
R² = 0.0193
y = 1.2098x - 11.265
R² = 0.4812
y = -0.3902x + 55.608
R² = 0.1417
y = -0.5955x + 67.853
R² = 0.2674
Normoxia DMSO/AZ
Normoxia Rv/AZ
Hypoxia DMSO/AZ
Hypoxia Rv/AZ
Linear (Normoxia DMSO/AZ)
Linear (Normoxia Rv/AZ)
Linear (Hypoxia DMSO/AZ)
Linear (Hypoxia Rv/AZ)

Figure S. 5

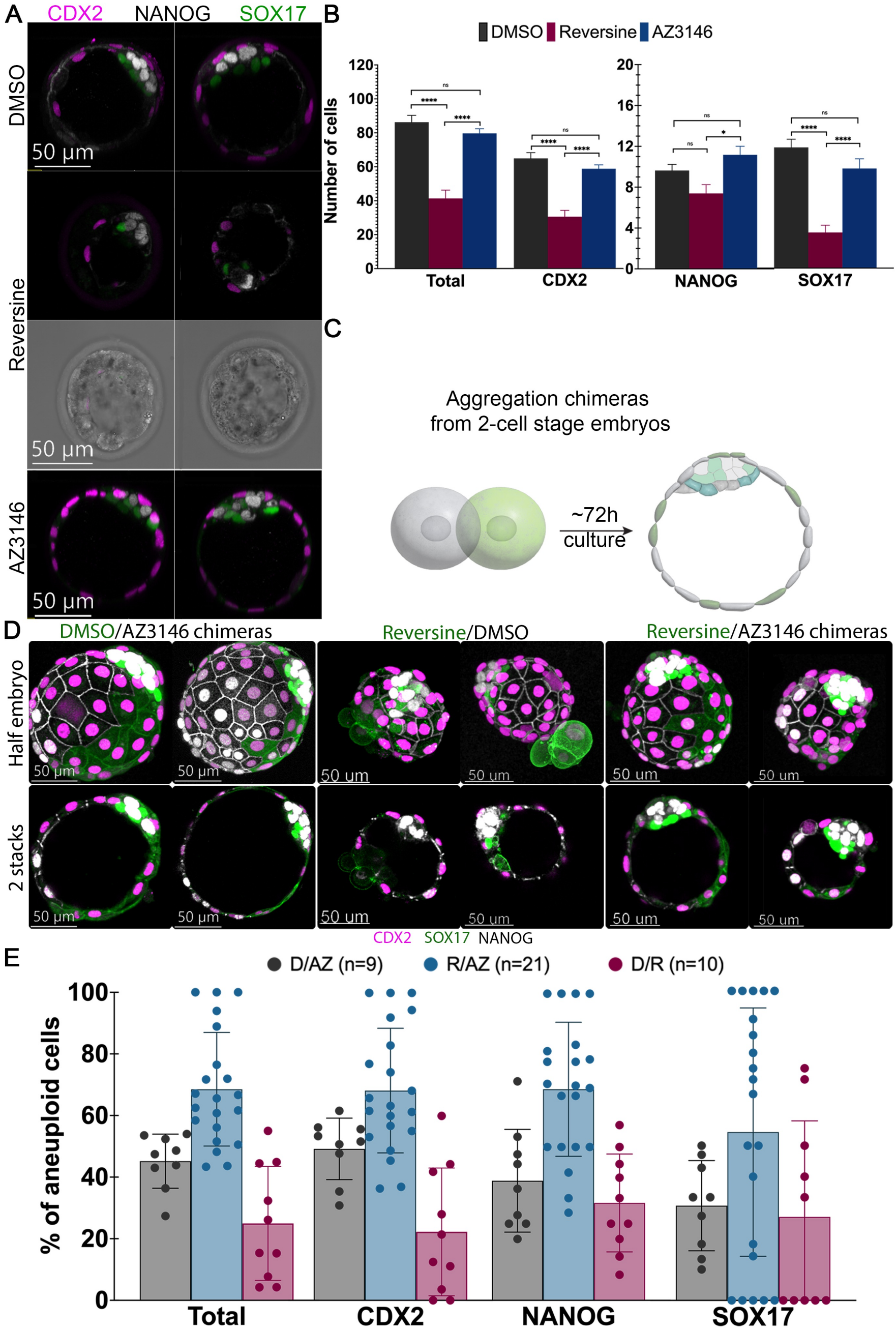
A
CDX2
NANOG
SOX17
DMSO
Reversine
AZ3146
50 µm
B
DMSO
Reversine
AZ3146
Number of cells
Total
CDX2
NANOG
SOX17
C
Aggregation chimeras
from 2-cell stage embryos
~72h
culture
Reversine/DMSO
Reversine/AZ3146 chimeras
D
DMSO/AZ3146 chimeras
Half embryo
2 stacks
50 um
E
CDX2
SOX17
NANOG
D/AZ (n=9)
R/AZ (n=21)
D/R (n=10)
% of aneuploid cells
Total
CDX2
NANOG
SOX17

Figure S. 6

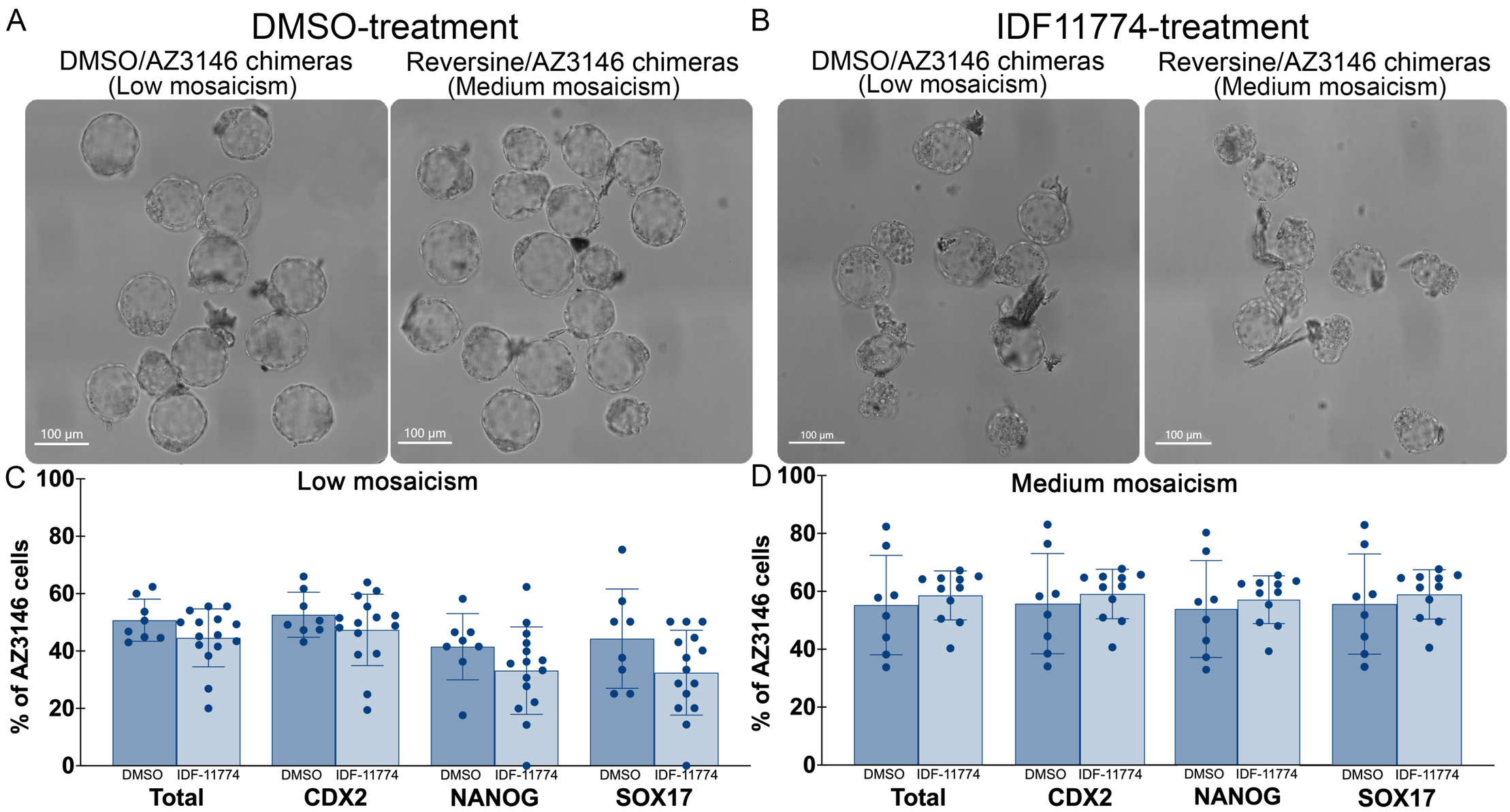
A
DMSO-treatment
DMSO/AZ3146 chimeras
(Low mosaicism)
Reversine/AZ3146 chimeras
(Medium mosaicism)
100 µm
100 µm
B
IDF11774-treatment
DMSO/AZ3146 chimeras
(Low mosaicism)
Reversine/AZ3146 chimeras
(Medium mosaicism)
100 µm
100 µm
C
Low mosaicism
% of AZ3146 cells
100
80
60
40
20
0
DMSO
IDF-11774
Total
CDX2
NANOG
SOX17
D
Medium mosaicism
% of AZ3146 cells
100
80
60
40
20
0
DMSO
IDF-11774
Total
CDX2
NANOG
SOX17